https://ntrs.nasa.gov/search.jsp?R=19930088152 2020-06-17T11:47:54+00:00Z

CONFIDENTIAL

Copy 375
RM L54B24

NACA RM L54B24

NACA

RESEARCH MEMORANDUM

TRANSONIC AERODYNAMIC AND LOADS CHARACTERISTICS OF A 4-PERCENT-THICK UNSWEPT-WING—FUSELAGE COMBINATION

By Gerald Hieser, James H. Henderson, and John M. Swihart

Langley Aeronautical Laboratory
Langley Field, Va.

CLASSIFICATION CHANGED TO UNCLASSIFIED
AUTHORITY: NASA PUBLICATIONS ANNOUNCEMENT NO. 7
EFFECTIVE DATE: MAY 29, 1959
WHL

CLASSIFIED DOCUMENT

This material contains information affecting the National Defense of the United States within the meaning of the espionage laws, Title 18, U.S.C., Secs. 793 and 794, the transmission or revelation of which in any manner to an unauthorized person is prohibited by law.

NATIONAL ADVISORY COMMITTEE
FOR AERONAUTICS

WASHINGTON

May 24, 1954

CONFIDENTIAL

NATIONAL ADVISORY COMMITTEE FOR AERONAUTICS

RESEARCH MEMORANDUM

TRANSONIC AERODYNAMIC AND LOADS CHARACTERISTICS OF A 4-PERCENT-THICK UNSWEPT-WING—FUSELAGE COMBINATION

By Gerald Hieser, James H. Henderson, and John M. Swihart

SUMMARY

An investigation has been conducted in the Langley 16-foot transonic tunnel to determine the basic aerodynamic and loading characteristics of an unswept-wing—fuselage combination employing a wing with aspect ratio 4, taper ratio 0.5, and NACA 65A004 airfoil sections. Force, moment, and pressure measurements were obtained at Mach numbers from 0.60 to 1.05 and angles of attack, depending on Mach number, from 0° to about 19°. The Reynolds number, based on mean aerodynamic chord, varied from 4.6×10^6 to 6.0×10^6.

Results of the investigation indicate that the aerodynamic-center position at zero lift shifts from 14.2 percent of the mean aerodynamic chord at a Mach number of 0.60 to 29.8 percent at a Mach number of 1.05.

Extensive wing pressure-distribution measurements show the existence of several major shocks on the wing at transonic speeds. The aerodynamic properties of the model are closely associated with the behavior of these shocks. The pressure distributions also show that the wing maintains negative leading-edge pressure peaks at moderate angles of attack throughout the Mach number range from 0.60 to 1.05. The variation of spanwise center of loading with Mach number and angle of attack was usually not more than 5 percent of the wing semispan. The drag-due-to-lift parameter decreases slightly, reaches a minimum value of 0.155 at a Mach number of 0.88, and then increases to a maximum value of 0.20 at a Mach number of 1.05.

INTRODUCTION

Thin unswept wings possess certain characteristics which are desirable for airplanes and missiles designed for supersonic flight. The most predominant of these characteristics are high lift-curve slope and potential structural simplicity.

Although many research programs at the National Advisory Committee for Aeronautics laboratories include investigations of the basic supersonic characteristics of thin unswept wing configurations, very little information is available concerning the changes in aerodynamic and loading characteristics in the transonic speed range. The available information includes the transonic drag rise at low lift for a number of unswept-wing—fuselage configurations (refs. 1 and 2) and the transonic lift, drag, and pitching-moment characteristics of a number of small-scale unswept wings (refs. 3 and 4).

A research program has been initiated at the Langley 16-foot transonic tunnel for the purpose of investigating the steady-state aerodynamic and loading characteristics, the effectiveness of lateral controls, the horizontal-tail effectiveness, the fluctuating flow properties, and the fluctuating loads on an unswept-wing—fuselage combination at transonic speeds and high Reynolds numbers. The results of the steady-state aerodynamic and loads investigation are presented in this paper.

The wing, which was mounted on a sting-supported fuselage, has zero sweep of the 0.50-chord line, taper ratio of 0.5, aspect ratio of 4, and NACA 65A004 airfoil sections.

The model was tested at Mach numbers from 0.60 to 1.06 and angles of attack from 0° to about 19°. The Reynolds number based on the wing mean aerodynamic chord varied from 4.6×10^6 to 6.0×10^6.

SYMBOLS

C_L lift coefficient, $\frac{\text{Lift}}{qS}$

C_N model normal-force coefficient, $\frac{\text{Model normal force}}{qS}$

$C_{N'}$ normal-force coefficient of wing panel outboard of 15.9-percent-semispan station, $0.815C_N \frac{S}{S'}$

C_D drag coefficient, $\frac{\text{Drag}}{qS}$

C_m pitching-moment coefficient,

$$\frac{\text{Pitching moment about mean aerodynamic quarter chord}}{qS\bar{c}}$$

ΔC_D total drag coefficient minus drag coefficient at zero lift

$\frac{d\Delta C_D}{dC_L^2}$ drag-due-to-lift parameter

$\left(\frac{L}{D}\right)_{max}$ maximum lift-drag ratio

C_{L_α} lift-curve slope per radian (average from $C_L = 0$ to $C_L = 0.4$)

C_{BM} wing-panel bending-moment coefficient,

$$\frac{4 \text{ (bending moment of wing panel outboard of 15.9-percent-semispan station)}}{qS'b'}$$

c_n section normal-force coefficient,

$$\int_0^1 \left(p_l - p_u\right) d\frac{x}{c}$$

$c_n\frac{c}{\bar{c}}$ section normal-load coefficient

P pressure coefficient, $\frac{p - p_o}{q}$

P_b base pressure coefficient, $\frac{p_b - p_o}{q}$

P_{cr} critical pressure coefficient

p local static pressure

p_o static pressure of undisturbed stream

M free-stream Mach number

q free-stream dynamic pressure

R Reynolds number based on $\bar{c}$

S wing area

S' wing-panel area, area of wing outboard of 15.9 percent semispan

c wing chord at any spanwise station

$\bar{c}$ mean aerodynamic chord, $\frac{2}{S}\int_0^{b/2} c^2 dy$

x longitudinal distance measured from nose of fuselage or wing leading edge

y lateral distance measured perpendicular to plane of symmetry

l body length

$\frac{\bar{y}}{b'/2}$ spanwise center of load parameter, $\frac{C_{BM}}{C_{N'}}$

$\bar{y}$ lateral distance from 15.9-percent-semispan station to wing-panel center of loading

b wing span

b' span of wing panels from 15.9-percent-semispan stations to tips

α angle of attack of model (fuselage reference line), deg

Λ sweep angle, deg

ϕ meridian angle from top of fuselage (looking forward)

Subscripts:

u upper

l lower

b inside fuselage, 2 inches forward from base of fuselage

MODEL AND APPARATUS

Model.- The geometric details of the model, including a table of the fuselage ordinates, are given in figure 1. The steel wing was mounted in a midwing position on the fuselage and had no geometric incidence, twist, or dihedral. The fuselage consists of a cylindrical body of revolution, an ogival nose, and a slightly boattailed afterbody. The ratio of the base

diameter to the maximum diameter is 0.66. A photograph of the model mounted in the Langley 16-foot transonic tunnel is shown as figure 2.

Instrumentation.- The forces and moments on the model were measured by a six-component internal strain-gage balance. The model angle of attack was obtained from the static angle of attack corrected for deflections due to load. These deflections, which occurred in the balance and sting, were determined from static calibrations under applied normal loads and pitching moments.

Fuselage pressure measurements were obtained along the 0° and 180° meridians from 0 percent to 78 percent of the fuselage length and along the 22.5° and 180° meridians from 82 percent to 98 percent of the fuselage length. Wing pressure orifices were located at 13.9 percent, 37.5 percent, and 77.7 percent of the semispan. At the innermost wing station, the orifices were installed on the fuselage about 1/16 inch from the wing surface. The wing and fuselage orifice locations are given in figure 1.

The wing-panel bending moment was obtained from a calibrated strain gage mounted at the 15.9-percent-semispan station on the surface of the left wing.

The model base pressures were measured by two orifices mounted flush with the internal surface of the fuselage about 2 inches from the fuselage base.

Tunnel and model support.- The Langley 16-foot transonic tunnel, in which the tests were conducted, has an octagonal slotted test section permitting a continuous variation in speed to Mach numbers slightly above 1.0.

The sting-support system, which is described in reference 5, is arranged so that the model is located near the center of the tunnel at all angles of attack.

TESTS

Simultaneous measurements of the model forces, moments, and pressures were obtained for the Mach number and angle-of-attack range given in the following table:

Mach number	Angle-of-attack range, deg
0.60	0 to 16.1
.70	0 to 16.3
.80	0 to 13.4
.85	0 to 16.6
.88	0.3 to 18.8
.90	0 to 16.8
.92	0.3 to 16.9
.94	0 to 15.2
.96	0 to 15.2
.98	0 to 15.2
1.00	0 to 13.1
1.04	0 to 7.6
1.05	0 to 7.5
1.06	0.3

The variation of the test Reynolds number (based on wing mean aerodynamic chord) with Mach number is given in figure 3.

ACCURACY

The measurement of Mach number in the test region is believed to be accurate within ± 0.005 (ref. 6). Corrections for airstream alinement, which were determined by testing the model in the upright and inverted positions, have been applied to the model angle of attack. The angles of attack presented are estimated to be correct within $\pm 0.1^{\circ}$.

The variation of model-base-pressure coefficient with angle of attack and Mach number is presented in figure 4. These data were used to adjust the lift and drag data to the condition of free-stream static pressure at the model base.

No adjustments for sting interference or aeroelasticity have been applied to the aerodynamic forces and moments. The maximum twist of the wing will occur when the product of normal force and distance from section center of gravity (considered to be flexural axis) to the center of pressure is a maximum. This product occurred at a Mach number of 0.80 and an angle of attack of about 7.5°. The maximum twist based on the measured chordwise and spanwise loading was estimated to be about 0.6° for the stated condition. It is believed that boundary-interference effects are generally negligible in this slotted test section (see ref. 7), and no attempt to correct the data for these effects has been made. The accuracy

of the measured coefficients based on balance accuracy and repeatability of data is believed to be within the following limits:

C_L	± 0.01
C_D at low lift coefficients	± 0.001
C_D at high lift coefficients	± 0.003
C_m	± 0.003

TEST RESULTS

Wing and fuselage pressure distributions at representative Mach numbers and angles of attack are presented in figures 5 and 6, respectively. Sketches showing the positions of shocks on the wing at several conditions are given in figure 7. The lift, drag, and pitching moment, and wing-panel bending-moment characteristics for the Mach number and angle-of-attack range tested are presented in figures 8 to 11. Figures 12 to 20 present the analysis prepared from these data.

DISCUSSION

Aerodynamic Characteristics

Flow characteristics.- At Mach numbers from 0.60 to 0.80 and moderate angles of attack, the main compression shock of the wing occurs near the leading edge. (See figs. 5(a) to 5(c).) As the angle of attack is increased at Mach numbers of 0.60 and 0.70, the peaks are reduced in magnitude and the region of low pressure spreads chordwise and indicates that flow separation is beginning at the leading edge. Increasing the angle of attack at a Mach number of 0.80 causes the wing-compression shock to move rearward; however, a pressure peak at the leading edge still exists and indicates the presence of a weak oblique shock in this region. The oblique shock is probably associated with a transition from a laminar to a turbulent boundary layer. Inspection of the pressures at a Mach number of 0.85 (fig. 5(d)) reveals that the flow phenomena at moderate angles of attack are similar to the flow observed at higher angles of attack at a Mach number of 0.80. For example, compare the pressure distributions for $M = 0.80$ and $\alpha = 5.02^\circ$ with the pressure distributions for $M = 0.85$ and $\alpha = 2.70^\circ$.

Some interesting features of the shock behavior and flow about the wing at transonic speeds are revealed by the pressure distributions obtained at Mach numbers of about 0.88 and above (figs. 5(e) to 5(l).) In order to illustrate the locations of the shocks and their movement

with increasing Mach number and angle of attack, sketches of the positions of the shocks are shown in figure 7 for several conditions. The shock positions are indicated only over the portion of the wing semispan where they can be definitely located from the pressure distributions.

The main compression shock of the wing usually extends along a constant percent chord line and moves rearward with increasing Mach number and angle of attack. At a Mach number of about 0.96, this shock has reached the wing trailing edge except at very low angles of attack. (See fig. 5(i).)

The oblique shock in the region of the leading edge, which was previously mentioned in the discussion of the flow at lower speeds, exists throughout the transonic speed range. (See figs. 5(e) to 5(l).) The isobars shown in figure 7 indicate that this shock probably does not extend inward to the fuselage wing juncture. The leading-edge negative pressure peaks associated with this oblique shock exist at moderate angles of attack throughout the Mach number range even though the wing leading edge is slightly forward of the Mach line at Mach numbers of 1.04 and 1.05. It has also been shown in reference 8 that leading-edge pressure peaks have been obtained for a 40° sweptback wing at a Mach number of 1.59, in which case the wing leading edge was also slightly forward of the Mach line. Apparently, the existence of leading-edge pressure peaks is possible at the highest Mach numbers presented herein because of the subsonic nature of the flow in the immediate vicinity of the leading edge. Since the wing has thickness, a detached shock (bow wave) must be expected on the basis of two-dimensional considerations and therefore the normal flow component at the leading edge will be subsonic. (See ref. 9.)

The crossmarks shown at the 37.5-percent-semispan station in figure 7 designate the location of a weak oblique shock indicated on the pressure distributions at Mach numbers from 0.88 to 1.05. (See figs. 5(e) to 5(l).) This shock probably results from a disturbance from the wing leading-edge fuselage juncture and, as indicated by the isobars of figure 7, probably exists along a line extending inward toward the vicinity of the juncture. The oblique shock noted at the 77.7-percent-semispan station at Mach numbers from 0.90 to 1.05 (figs. 5(f) to 5(l).) also indicated by crossmarks in figure 7, probably results from a disturbance at the wing-tip leading edge. Both of these shocks move rearward with increasing angle of attack but their positions are unaffected by changes in Mach number. The locations of these two shocks predicted by utilizing the pressures just ahead of the shocks agree well with the positions shown by the pressure distributions.

Lift characteristics.- The lift curves of figure 8 show that, at Mach numbers from 0.80 to 0.90, the lift-curve slope increases with increasing angle of attack in the lift-coefficient range from 0 to about 0.60. This

increase in slope is due to the rearward movement of the main wing shock with increasing angle of attack. (See figs. 5(c) to 5(f).)

The maximum lift coefficient at a Mach number of 0.60 is about 0.80, whereas at a Mach number of 0.92 this value increases to about 1.1. (See fig. 8.) At higher Mach numbers the maximum lift coefficient was not reached because of the limitations of model strength but a lift coefficient of 1.3 was attained at $M = 0.94$, and there was no indication of stall.

Drag characteristics.- The variation of drag coefficient with Mach number for several values of lift coefficient is presented in figure 12. The decrease in drag experienced at Mach numbers near 0.88 and lift coefficients from about 0.20 to 0.40 is associated with the main wing shock position. As can be seen from the wing pressure distributions of figure 5 and shock diagrams of figure 7, the shock at a Mach number of about 0.88 is located near the wing maximum thickness resulting in large negative pressures over the entire forward portion of the wing, so that there is a reduction in the pressure drag. With increasing Mach number, the drag increases since the rearward movement of the shock results in large negative pressures over progressively greater portions of the wing back of the maximum thickness until the shock reaches the wing trailing edge at a Mach number of about 0.96. Inspection of the wing pressure distributions (fig. 5) reveals only slight changes in the wing pressures from a Mach number of 0.96 to 1.05 and results in a reduction in the rate of increase of the wing pressure drag with Mach number. The greater rate of increase in drag coefficient with Mach number at Mach numbers above 0.98 is caused primarily by the progressive decrease in pressures over the boattailed (78 percent to 100 percent of the body length) portion of the body. (See fig. 6(e).)

The drag-due-to-lift parameter was determined from the curves of ΔC_D plotted against C_L^2 obtained at lift coefficients from 0 to 0.40 as shown in figure 13. The value of this parameter, which is presented in figure 14, decreases slightly, reaches a minimum value of 0.155 at a Mach number of 0.88, and then increases to a maximum value of 0.20 at a Mach number of 1.05. Also shown in figure 14 is the value of $1/C_{L_\alpha}$ which predicts the drag due to lift based on the assumption that the chord force is zero. A comparison of the experimental curve with the predicted shows that, in the lift-coefficient range from 0 to 0.40, the chord force was less at lifting conditions than at zero lift at Mach numbers up to about 0.88. Since the experimental curve is higher than that predicted on the basis of the lift-curve slope at Mach numbers above 0.88, it is apparent that the chord force increased with increasing lift at these higher Mach numbers. Inspection of the wing and body pressure distributions of figures 5 and 6 reflects this behavior of the chord force. At Mach numbers below about 0.88, the rearward movement of

the main wing shock with increasing angle of attack decreased the chord force by decreasing the pressures ahead of the maximum thickness. The increasing chord force with increasing angle of attack at higher Mach numbers resulted from the following significant changes in the pressure distributions: Since the main wing shock was located back of the maximum thickness, further rearward shock movement with angle of attack decreased the pressures over the rear portion of the wing and thereby increased the chord force. Increased positive pressures on the wing lower surface ahead of the maximum thickness resulted from increasing angle of attack. Finally, at Mach numbers above about 0.98, the pressures over the boattailed portion of the body decreased slightly with increasing angle of attack.

The variation of maximum lift-drag ratio with Mach number shown in figure 15 indicates a reduction of about 50 percent in $(L/D)_{max}$ from subsonic speeds to the highest Mach number tested.

Pitching-moment characteristics.- The variation of pitching moment with lift coefficient (fig. 10) indicates large changes in the aerodynamic-center position at zero lift (15.6 percent of the mean aerodynamic chord) through the Mach number range. This total change from 14.2 percent $\bar{c}$ at a Mach number of 0.60 to 29.8 percent $\bar{c}$ at a Mach number of 1.05 results from changes in leading-edge pressure peaks and shock positions with Mach number as illustrated by the pressure distributions of figure 5.

The aerodynamic-center location determined from the present investigation agrees well with the data of reference 4 for a similar wing-fuselage combination. It is indicated in reference 4 that addition of the fuselage to the wing moved the aerodynamic-center position forward about 7 percent.

Presented in figure 16 is the variation of chordwise center of pressure with angle of attack for several Mach numbers. At Mach numbers from about 0.92 to 1.05, the chordwise center of pressure was generally located at about 33 percent $\bar{c}$ except at the low angles of attack where its position was farther forward. At Mach numbers from 0.60 to 0.90, the center-of-pressure position varied from about 13 percent $\bar{c}$ at low angles of attack to about 31 percent $\bar{c}$ at high angles of attack.

Inspection of the wing pressure distributions (fig. 5) indicates that the forward position of the chordwise center of pressure at the low angles of attack and Mach numbers of about 0.90 and lower is caused primarily by the large negative pressure peaks at the leading-edge region of the wing. At Mach numbers between 0.60 and 0.80, a large rearward shift in center of pressure occurs at moderate angles of attack because of upper-surface flow separation. A large rearward shift in the center of pressure resulting from a rearward movement of the main wing shock occurs at progressively lower angles of attack as the Mach number is

increased from about 0.85 to about 0.92. No large changes in the chordwise center-of-pressure location occur at Mach numbers above 0.92, since the main wing shock is located near the wing trailing edge throughout most of the angle-of-attack range.

Loading Characteristics

At high Mach numbers and angles of attack, the wing pressures (fig. 5) have chordwise distributions approaching a trapezoidal shape. These chordwise pressure distributions are similar in shape for the same Mach numbers to those found on wings of different thickness ratios or angles of sweep than the present wing (for instance, see refs. 10 and 11).

The variation of section normal-load coefficient (integrated section normal-force coefficient based on wing geometry) $c_n\frac{c}{\bar{c}}$ with model normal-force coefficient C_N is presented for various Mach numbers in figure 17. The zero-semispan-station normal-load coefficients were based on the wing root chord determined by extending the wing to the model plane of symmetry and were determined from the body orifices in this region. Inspection of figure 17 indicates that little change in the span-load distributions would occur with change in angle of attack except that the proportion of load over the fuselage station increases slightly at high angles of attack.

A theoretical spanwise loading distribution, which was estimated for a Mach number of 0.60 by use of the charts in reference 12, is compared in figure 18 with experimental section normal-load coefficients obtained from figure 17 for a model normal-force coefficient of 0.2. The experimental normal-load coefficients for a Mach number of 0.60 show that the wing-span-loading distribution outboard of the fuselage is essentially equal to the theoretical loading distribution. The normal-load coefficients shown for Mach numbers of 0.92 and 1.05 indicate only small variations in load distribution with Mach number outboard of the fuselage. The good agreement of the normal-load coefficients with the theoretical spanwise loading of reference 12 does not indicate that this simple theory can be used to predict other aerodynamic characteristics such as chordwise center-of-pressure location, lift-curve slope, pitching-moment coefficient, etc.

The spanwise center-of-load parameter $\frac{\bar{y}}{b'/2}$ is shown as a function of wing-panel normal-force coefficient and Mach number in figures 19 and 20, respectively. This parameter was determined from the wing-panel bending-moment and normal-force coefficients. In order to determine the panel normal-force coefficients, an estimation of the ratio of the normal load carried by the wing panel to the total model normal load was made

from the spanwise loading distributions. This ratio was found to be about 0.815 and was very nearly constant for all angles of attack and Mach numbers. Figure 19 indicates that the spanwise variation of the center of load with normal-force coefficient is less than 5 percent of the wing-panel semispan except for a few points beyond the stall. Figure 20 indicates that the spanwise variation of center of load with Mach number for a normal-force coefficient of 0.4 is only about 5 percent of the panel semispan.

CONCLUDING REMARKS

Results of an investigation to determine the transonic aerodynamic and loads characteristics of an unswept-wing—fuselage combination lead to the following general remarks:

Extensive wing pressure-distribution measurements show the existence of several major shocks on the wing at transonic speeds. The aerodynamic properties of the model are closely associated with the behavior of these shocks. The pressure distributions also show that the wing maintains leading-edge negative pressure peaks at moderate angles of attack throughout the Mach number range from 0.60 to 1.05.

The static longitudinal stability indicates large changes in the aerodynamic-center position (15.6 percent of the mean aerodynamic chord) throughout the Mach number range investigated. This total change (from 14.2 percent mean aerodynamic chord at a Mach number of 0.60 to 29.8 percent at a Mach number of 1.05) results from changes in the level and extent of the leading-edge pressure peaks and shock positions with Mach number.

The spanwise center of loading did not change more than 5 percent of the wing semispan throughout Mach number and angle-of-attack range except for some angles of attack beyond the stall.

The drag-due-to-lift parameter decreases slightly with increasing Mach number, reaches a minimum value of 0.155 at a Mach number of 0.88, and then increases to a maximum value of 0.20 at a Mach number of 1.05. A comparison of the measured drag due to lift with the values predicted by assuming that the chord force is zero indicates that, at Mach numbers below about 0.88, the chordwise force decreases with increasing lift up

to a lift coefficient of about 0.4, whereas above a Mach number of 0.88 the chordwise force increases with increasing lift.

Langley Aeronautical Laboratory,
National Advisory Committee for Aeronautics,
Langley Field, Va., February 3, 1954.

REFERENCES

1. Morrow, John D., and Nelson, Robert L.: Large-Scale Flight Measurements of Zero-Lift Drag of 10 Wing-Body Configurations at Mach Numbers From 0.8 to 1.6. NACA RM L52D18a, 1953.

2. Williams, Claude V.: A Transonic Wind-Tunnel Investigation of the Effects of Body Indentation, As Specified by the Transonic Drag-Rise Rule, on the Aerodynamic Characteristics and Flow Phenomena of an Unswept-Wing—Body Combination. NACA RM L52L23, 1953.

3. Nelson, Warren H., and McDevitt, John B.: The Transonic Characteristics of 17 Rectangular, Symmetrical Wing Models of Varying Aspect Ratio and Thickness. NACA RM A51A12, 1951.

4. Myers, Boyd C., II, and Wiggins, James W.: Aerodynamic Characteristics of a Wing With Unswept Quarter-Chord Line, Aspect Ratio 4, Taper Ratio 0.6, and NACA 65A004 Airfoil Section. Transonic-Bump Method. NACA RM L50C16, 1950.

5. Hallissy, Joseph M., and Bowman, Donald R.: Transonic Characteristics of a 45° Sweptback Wing-Fuselage Combination. Effect of Longitudinal Wing Position and Division of Wing and Fuselage Forces and Moments. NACA RM L52K04, 1953.

6. Ward, Vernon G., Whitcomb, Charles F., and Pearson, Merwin D.: Air-Flow and Power Characteristics of the Langley 16-Foot Transonic Tunnel With Slotted Test Section. NACA RM L52E01, 1952.

7. Whitcomb, Charles F., and Osborne, Robert S.: An Experimental Investigation of Boundary Interference on Force and Moment Characteristics of Lifting Models in the Langley 16- and 8-Foot Transonic Tunnels. NACA RM L52L29, 1953.

8. Cooper, Morton, and Spearman, M. Leroy: An Investigation of a Supersonic Aircraft Configuration Having a Tapered Wing With Circular-Arc Sections and 40° Sweepback. A Pressure-Distribution Study of the Aerodynamic Characteristics of the Wing at Mach Number 1.59. NACA RM L50C24, 1950.

9. Ferri, Antonio: Elements of Aerodynamics of Supersonic Flows. The MacMillan Co., 1949, p. 353.

10. Runckel, Jack F., and Henderson, James H.: A Correlation With Flight Tests of Results Obtained From the Measurement of Wing Pressure Distributions on a $\frac{1}{4}$-Scale Model of the X-1 Airplane (10-Percent-Thick Wing). NACA RM L52E29, 1952.

11. Loving, Donald L., and Estabrooks, Bruce B.: Transonic-Wing Investigation in the Langley 8-Foot High-Speed Tunnel at High Subsonic Mach Numbers and at a Mach Number of 1.2. Analysis of Pressure Distribution of Wing-Fuselage Configuration Having a Wing of 45° Sweepback, Aspect Ratio 4, Taper Ratio 0.6, and NACA 65A006 Airfoil Section. NACA RM L51F07, 1951.

12. DeYoung, John, and Harper, Charles W.: Theoretical Symmetric Span Loading at Subsonic Speeds for Wings Having Arbitrary Plan Form. NACA Rep. 921, 1948.

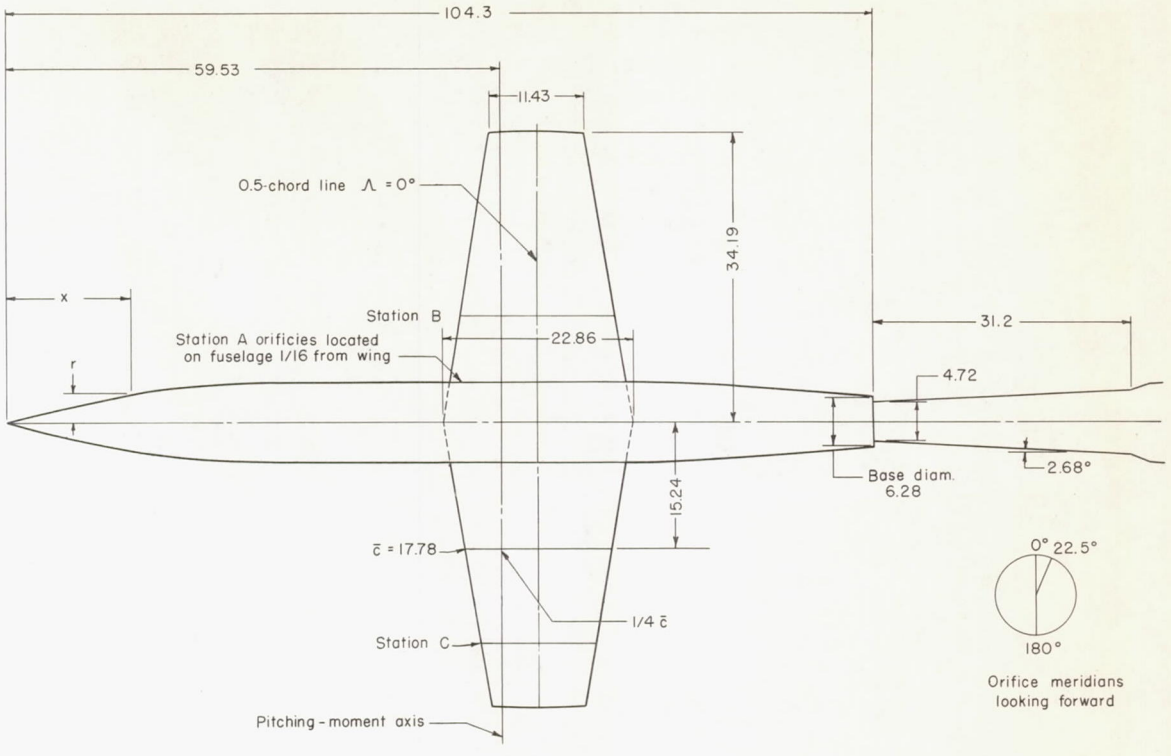

Fuselage ordinates			
x	r	x	r
0.000	0.000	24.000	4.396
0.500	0.144	26.000	4.536
1.000	0.286	28.000	4.643
1.500	0.426	30.000	4.716
2.000	0.564	32.000	4.755
3.000	0.832	33.333	4.763
4.000	1.091	78.582	4.763
5.000	1.341	79.000	4.757
6.000	1.582	79.250	4.752
7.000	1.812	79.500	4.746
8.000	2.035	80.000	4.728
9.000	2.249	80.500	4.708
10.000	2.454	81.000	4.685
10.500	2.551	81.916	4.639
11.000	2.649	83.500	4.557
11.625	2.766	85.250	4.458
12.000	2.834	87.000	4.345
14.000	3.182	88.000	4.278
16.000	3.493	89.000	4.209
18.000	3.770	90.965	4.067
19.000	3.896	97.362	3.624
20.000	4.014	104.300	3.143
22.000	4.223		

Wing data	
Aspect ratio	4.0
Taper ratio	0.5
Wing area	8.165 sq.ft.
Airfoil section	65A004

Wing orifice locations		
Spanwise station location, percent semispan		
A	13.9	
B	37.5	
C	77.7	
Location of each station percent chord		
0	25.00	65.00
1.25	30.00	70.00
2.50	35.00	75.00
5.00	40.00	80.00
7.50	45.00	85.00
10.00	50.00	90.00
15.00	55.00	95.00
20.00	60.00	

Fuselage orifice locations	
Percent length	Angle from top looking forward
2.00	0°, 180°
4.00	
8.00	
12.00	
20.00	
28.00	
34.00	
38.00	
42.00	
46.00	
50.00	
54.00	
58.00	
62.00	
66.00	
70.00	
74.00	
78.00	
82.00	22.5°, 180°
86.00	
90.00	
94.00	
98.00	

Figure 1.- Geometric details of model. All dimensions are in inches.

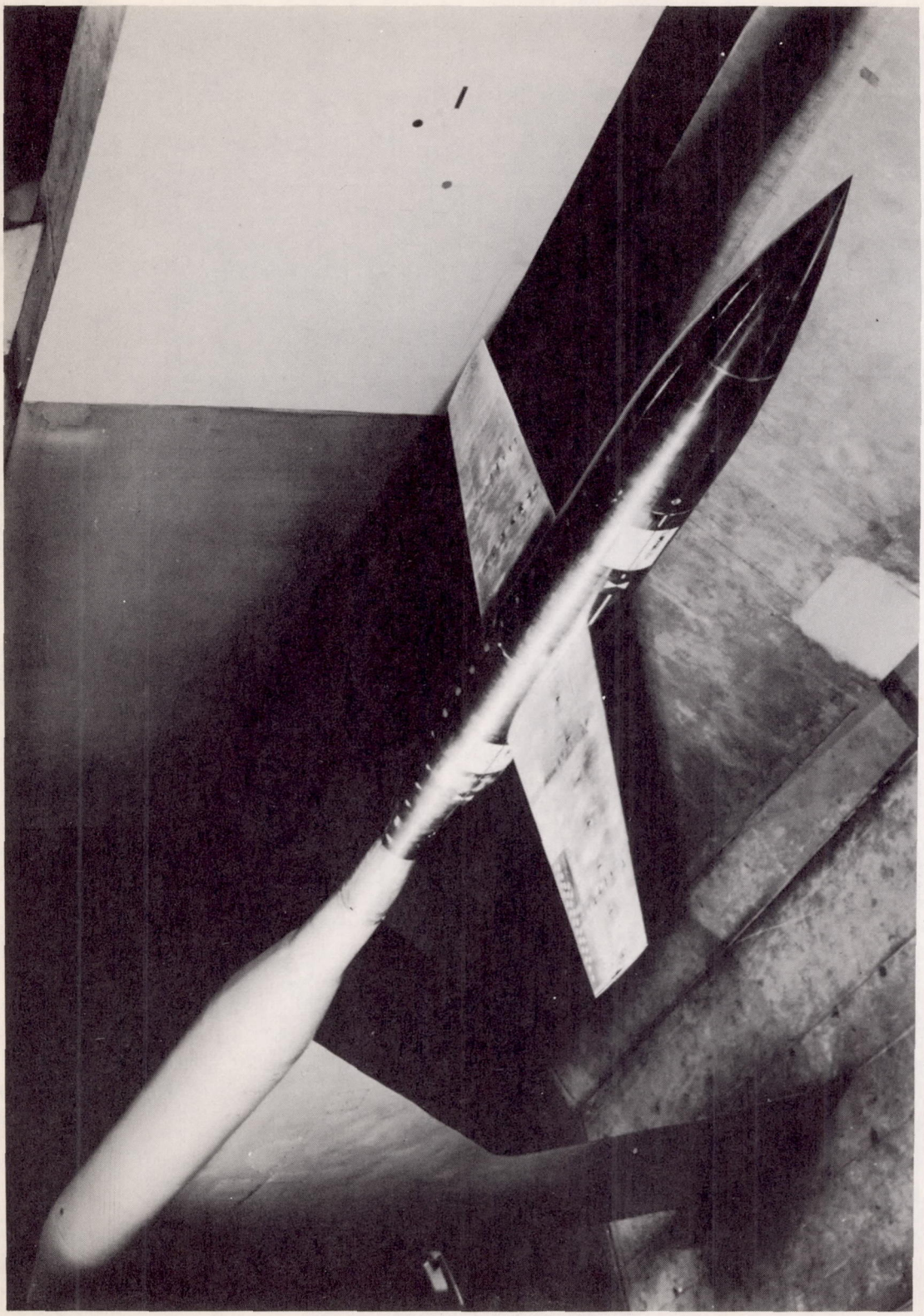

L-80813

Figure 2.- Photograph of the model mounted in the test section.

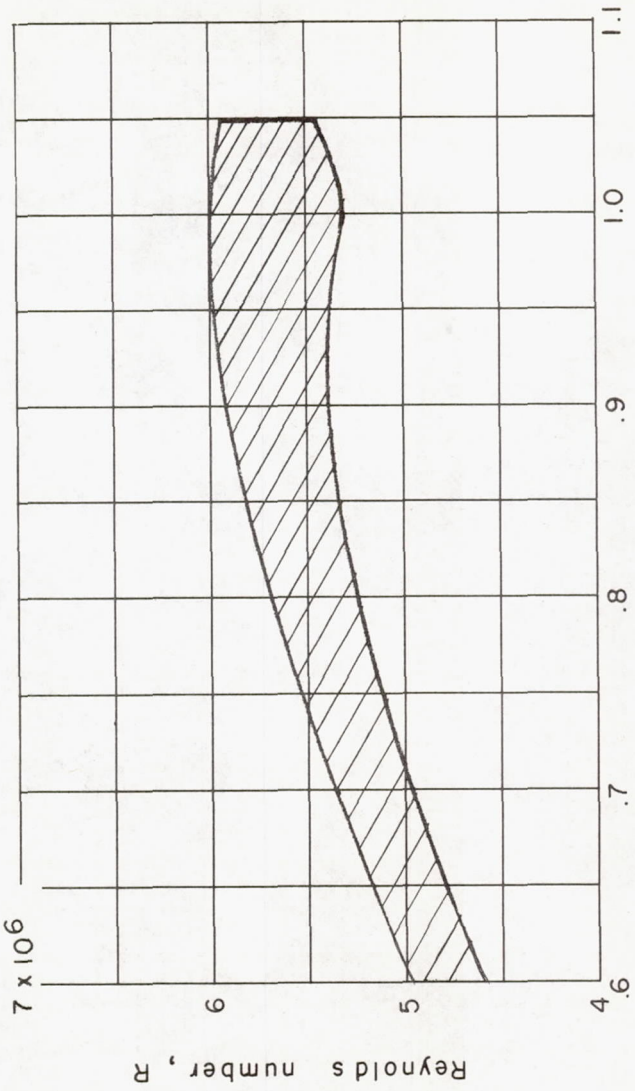

Figure 3.- Variation of Reynolds number with Mach number.

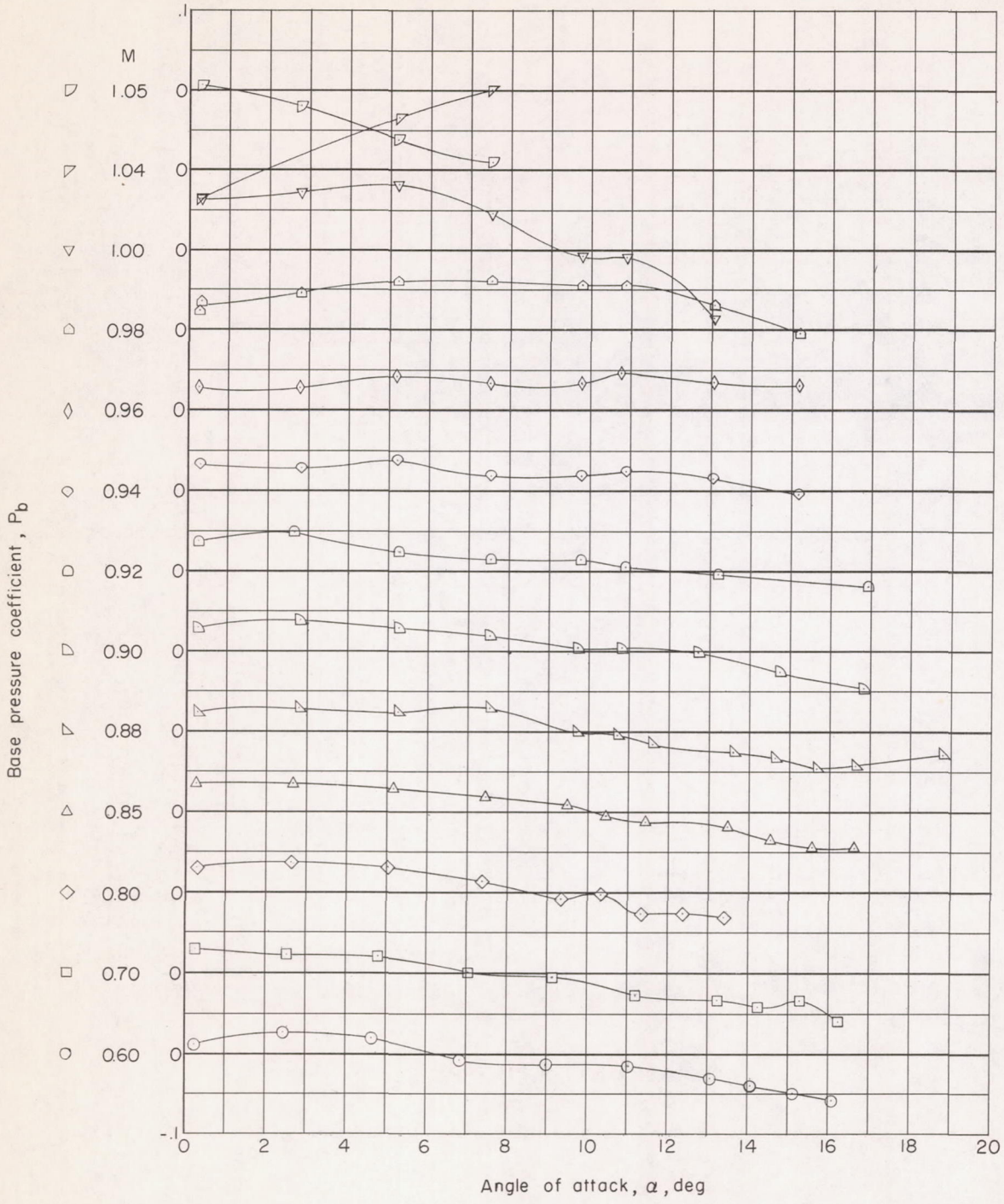

Figure 4.- Variation of base pressure coefficient with angle of attack for various Mach numbers.

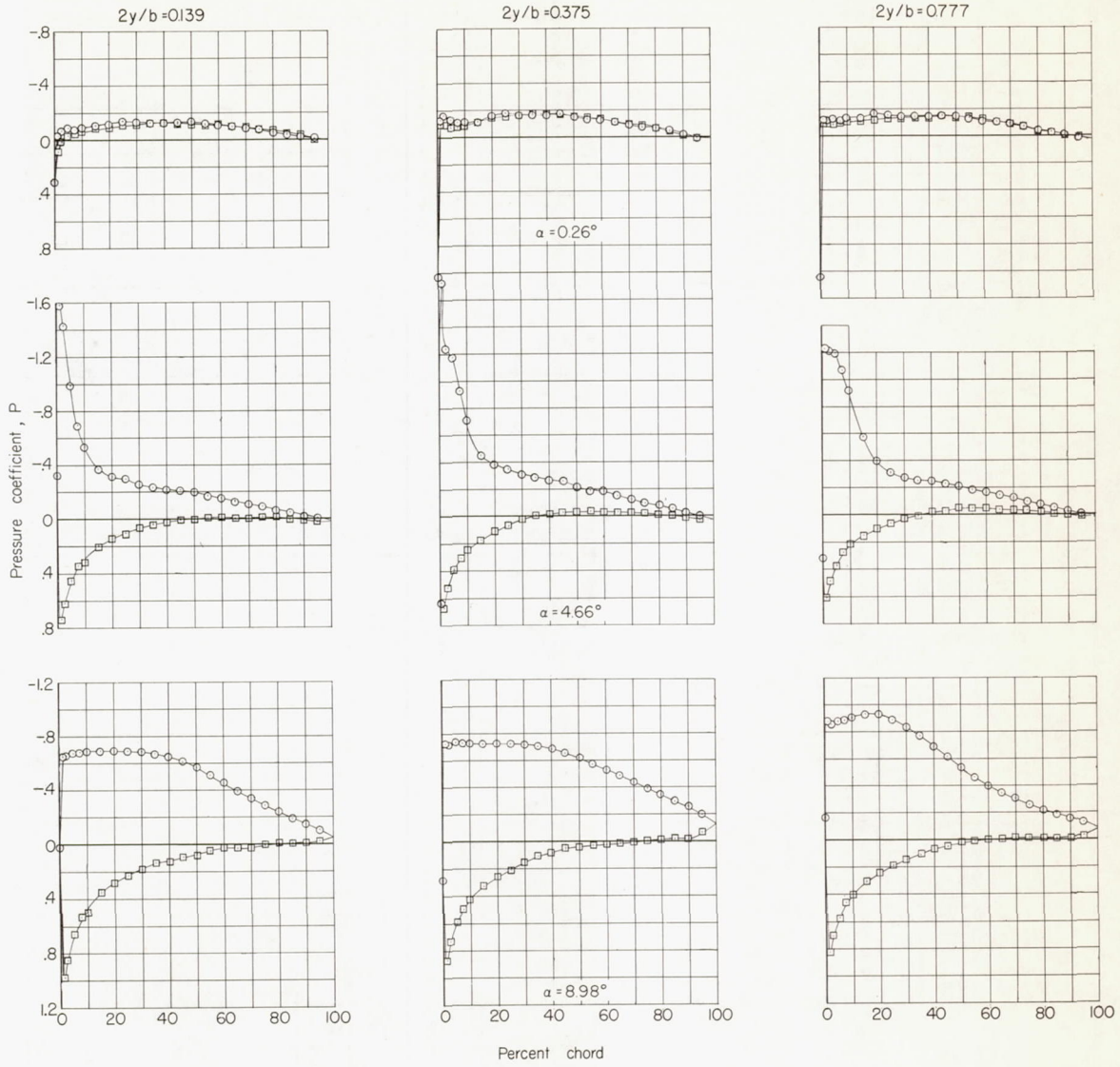

(a) M = 0.60; P_{cr} = -1.29

Figure 5.- Wing chordwise pressure distributions.

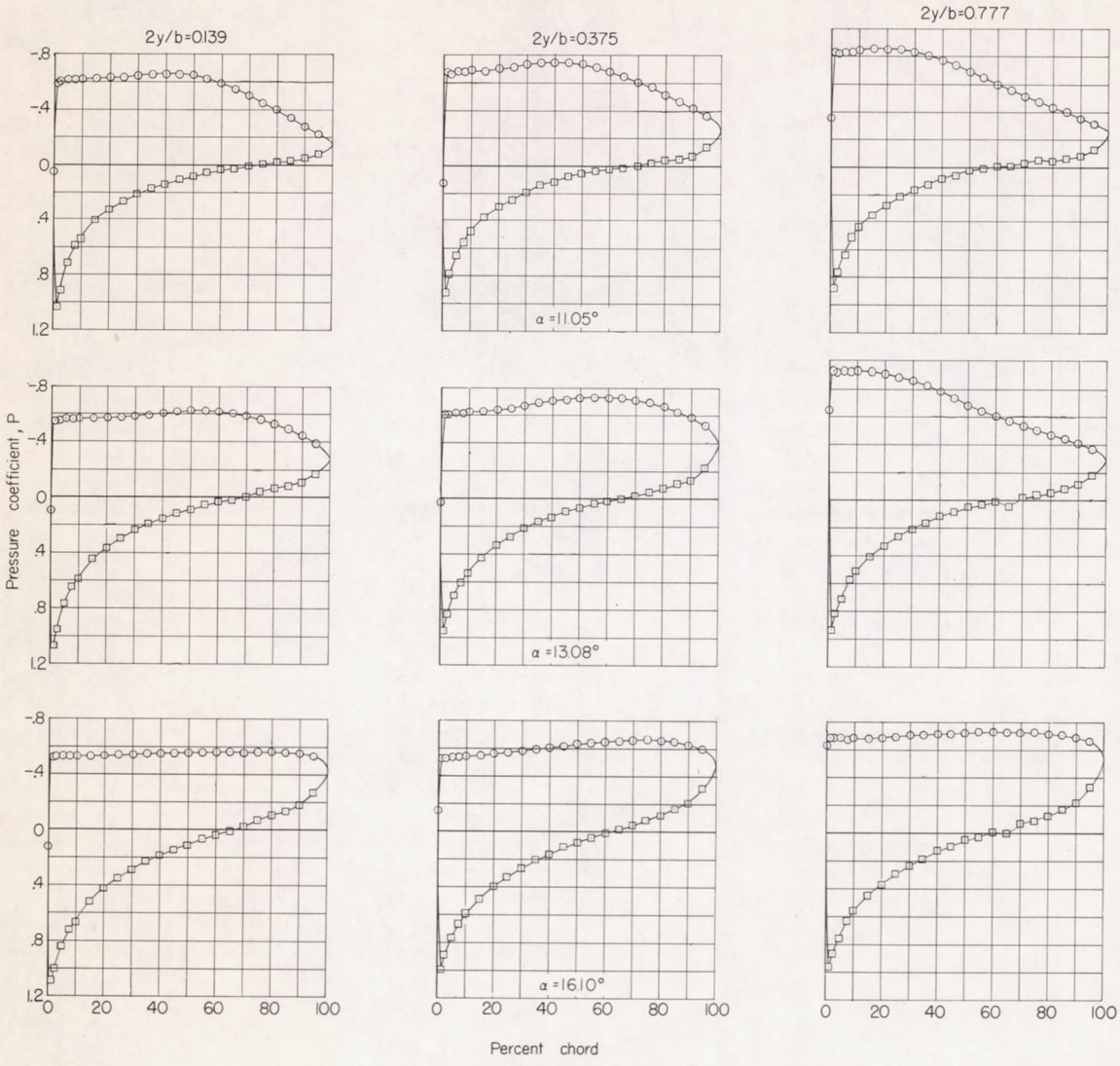

(a) Concluded.

Figure 5.- Continued.

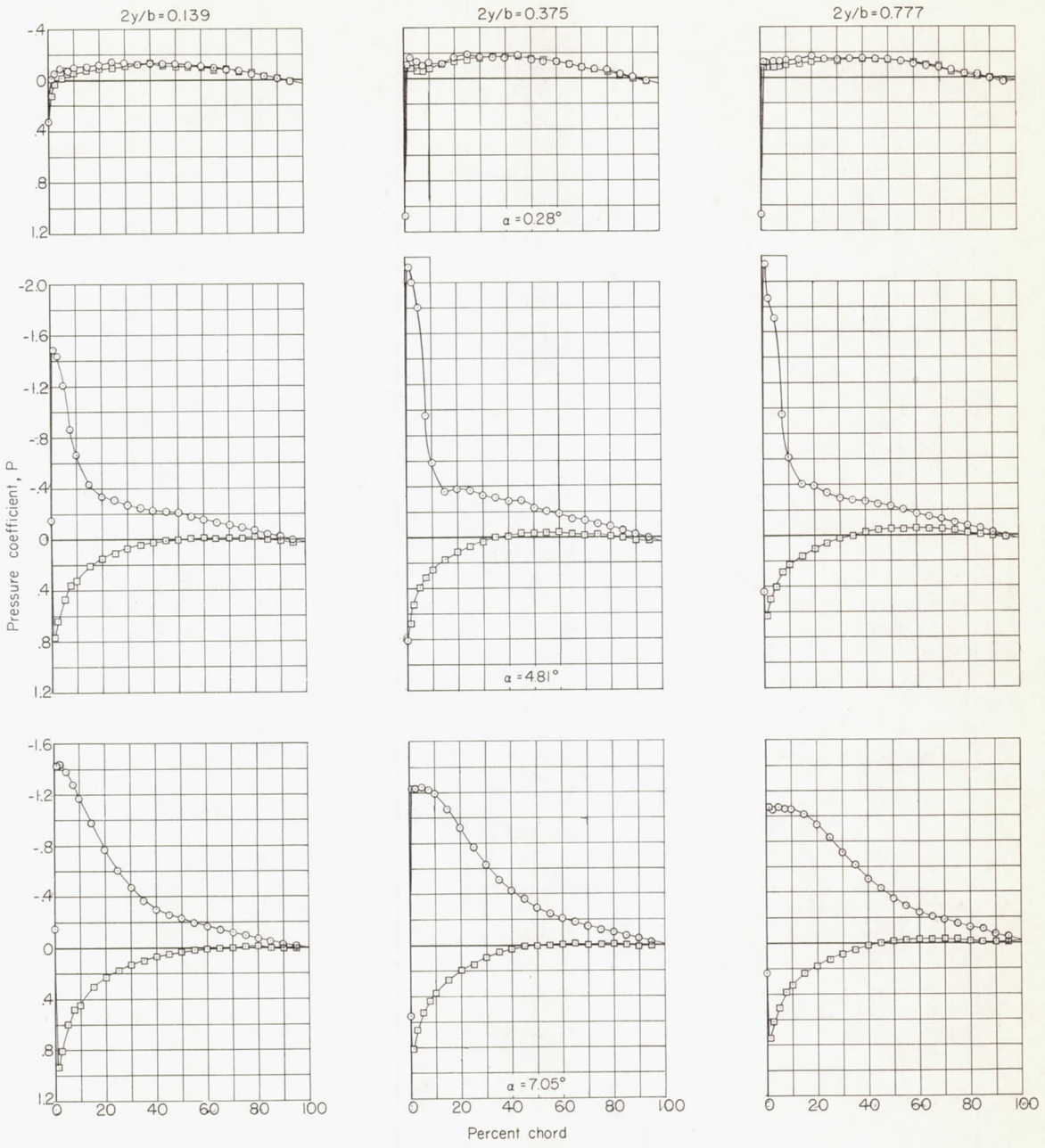

(b) M = 0.70; P_{cr} = -0.77.

Figure 5.- Continued.

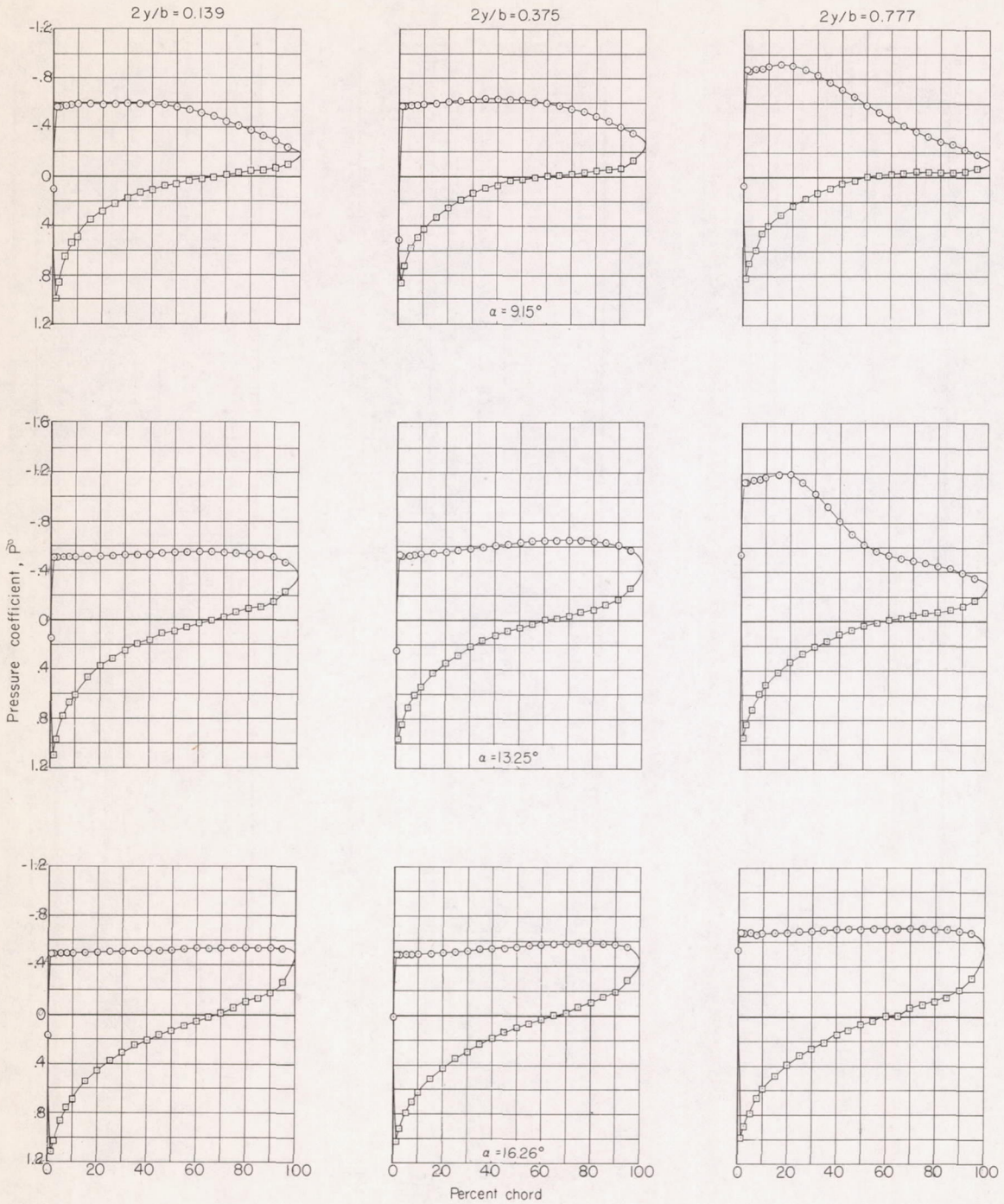

(b) Concluded.

Figure 5.- Continued.

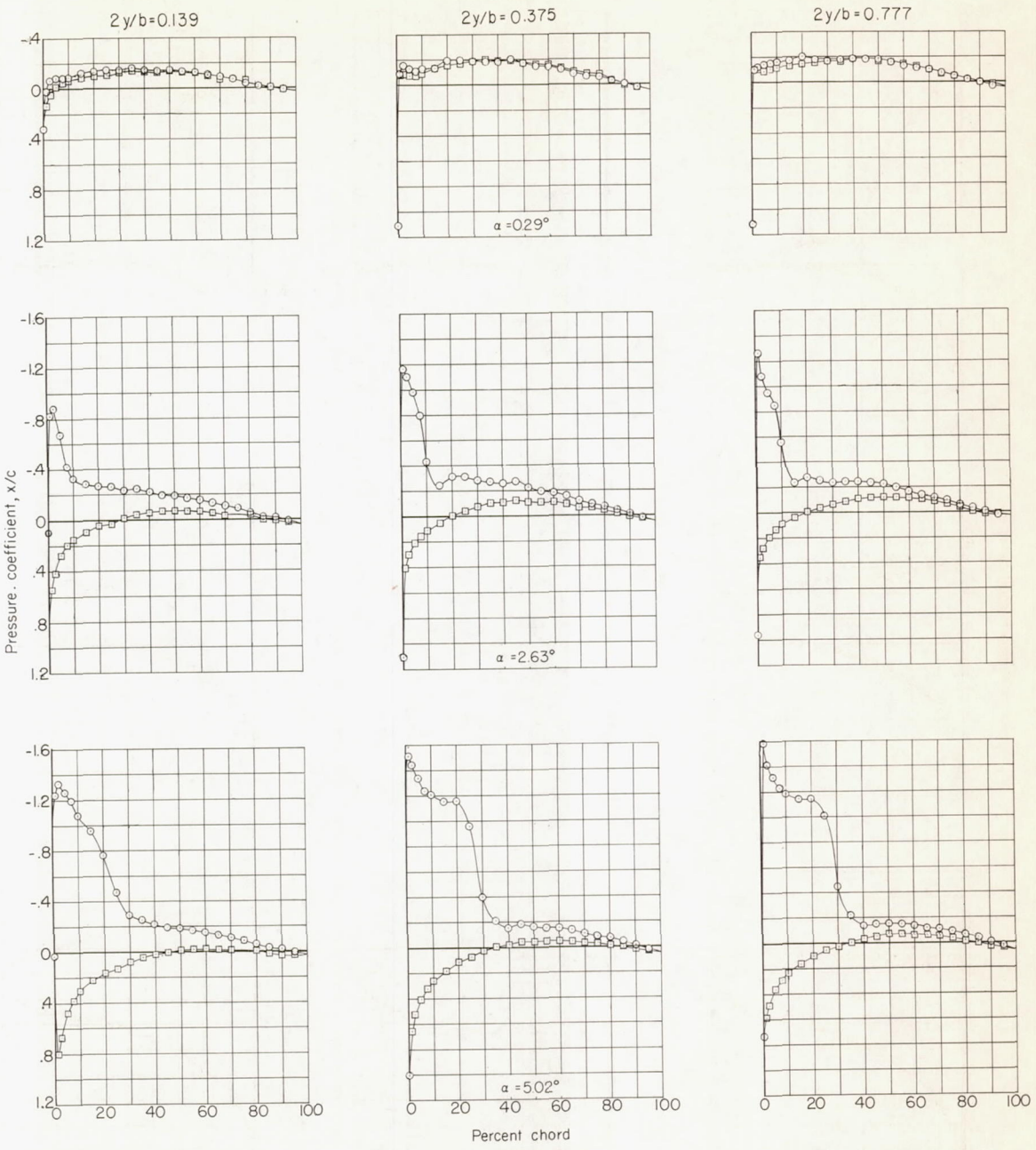

(c) M = 0.80; P_{cr} = -0.44.

Figure 5.- Continued.

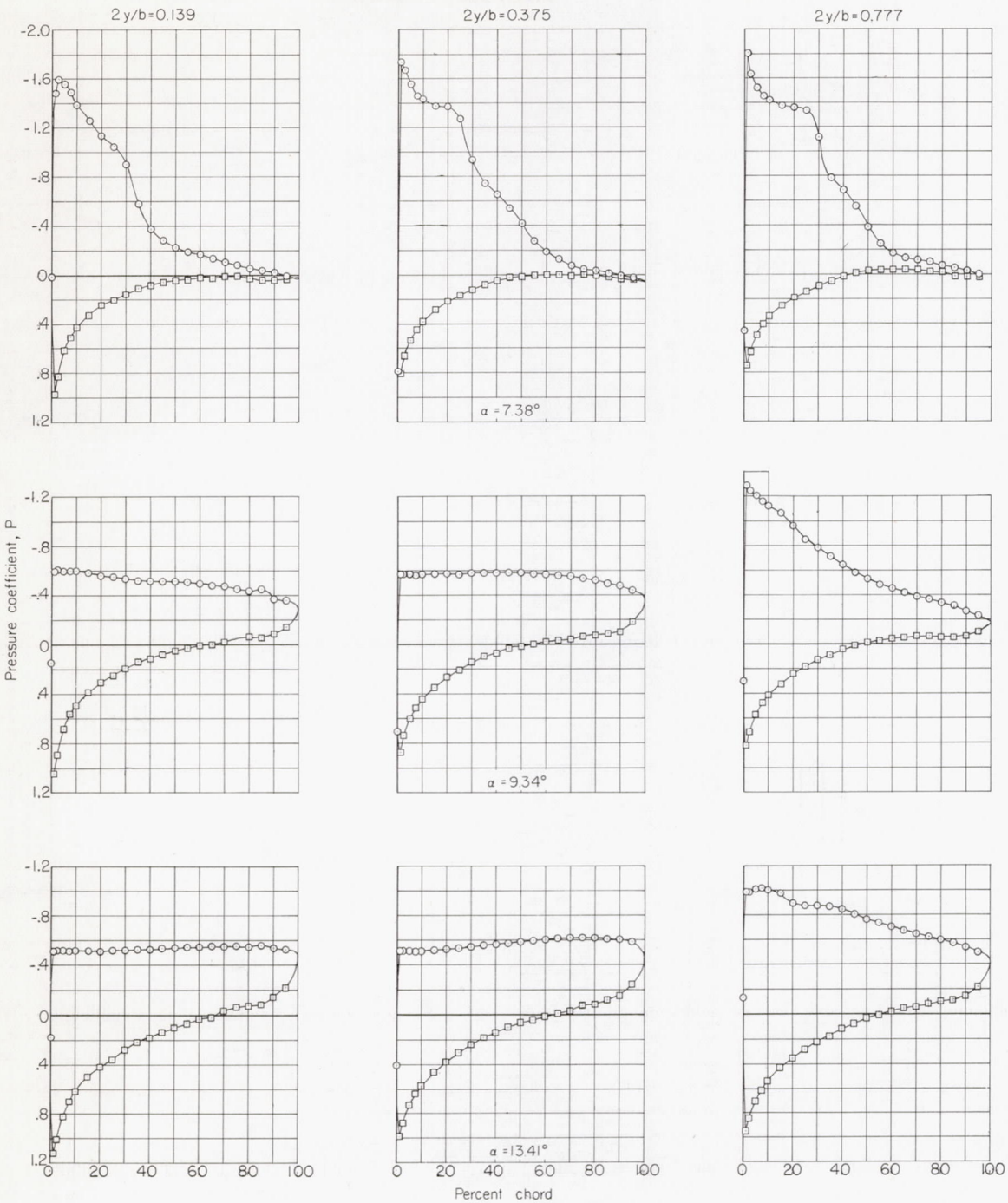

(c) Concluded.

Figure 5.- Continued.

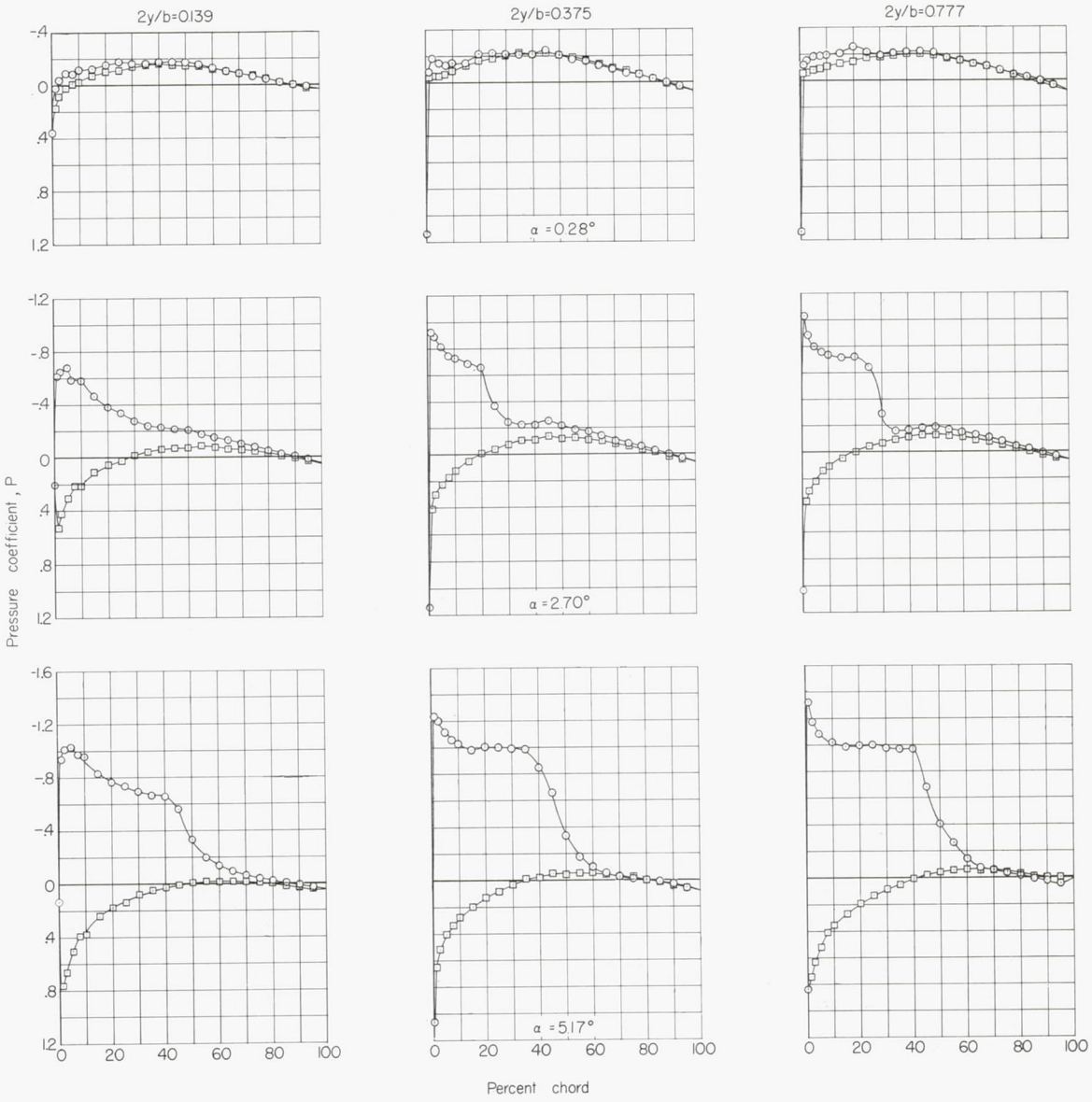

(d) M = 0.85; P_{cr} = -0.30.

Figure 5.- Continued.

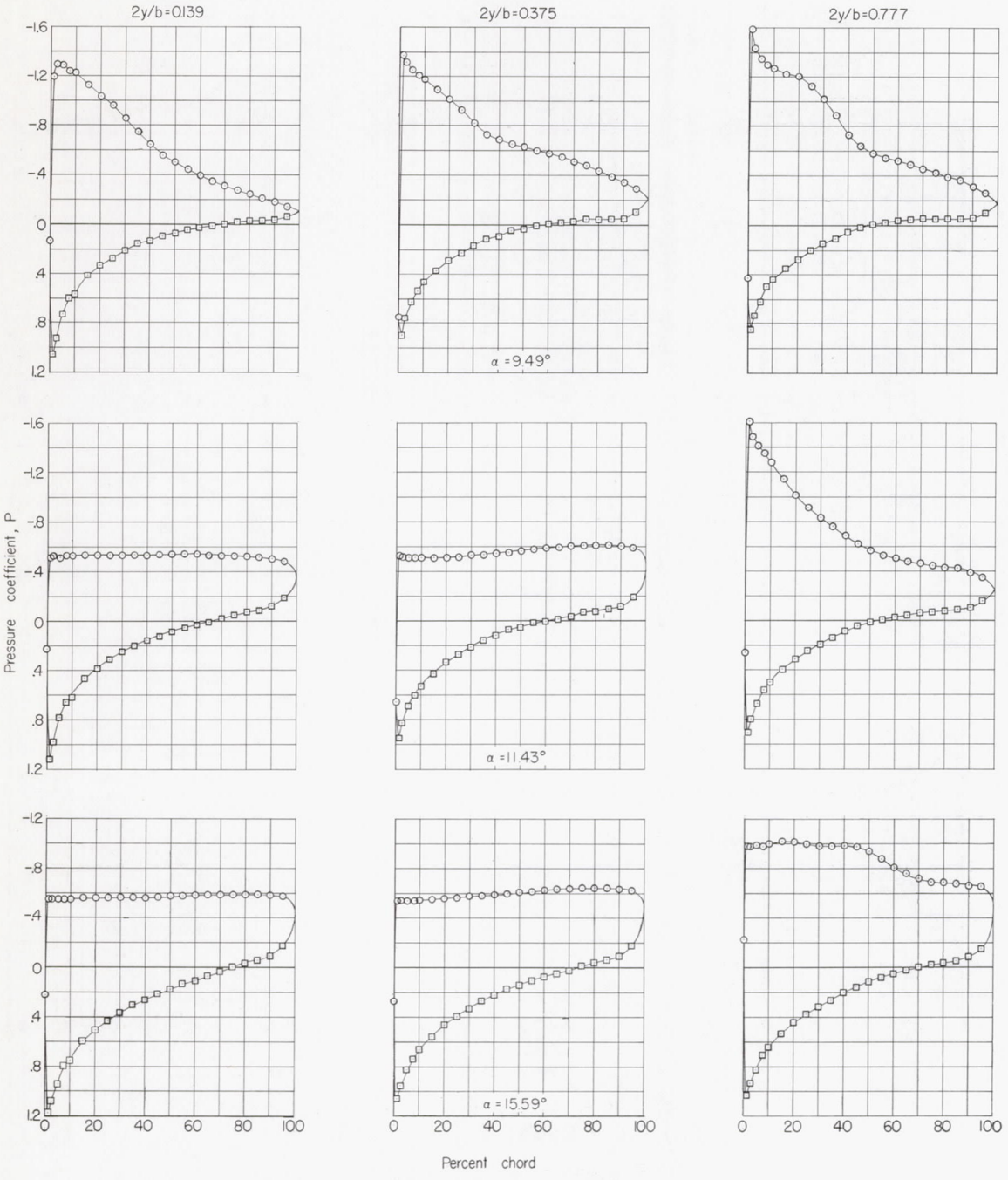

(d) Concluded.

Figure 5.- Continued.

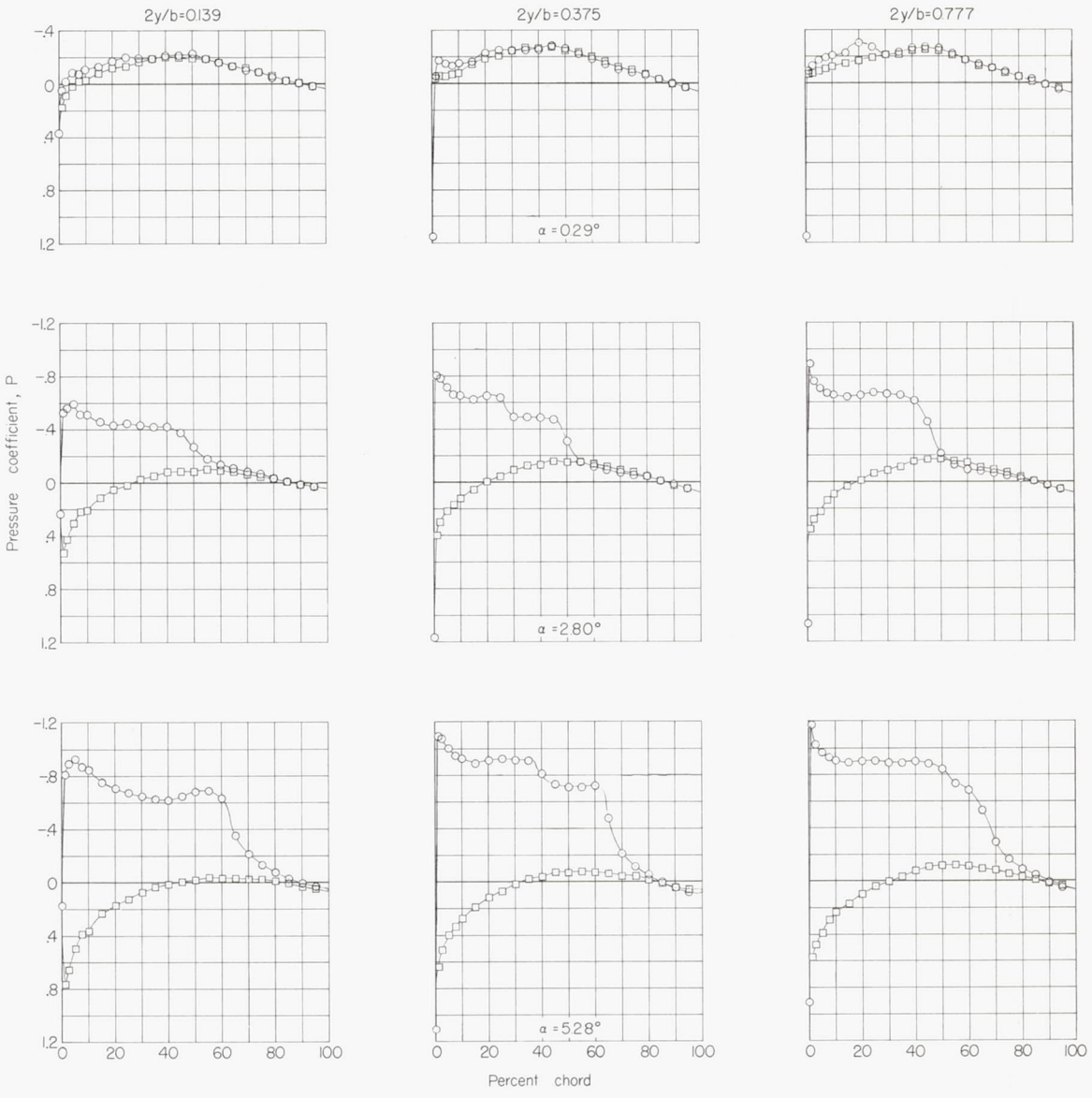

(e) M = 0.88; P_{cr} = -0.23.

Figure 5.- Continued.

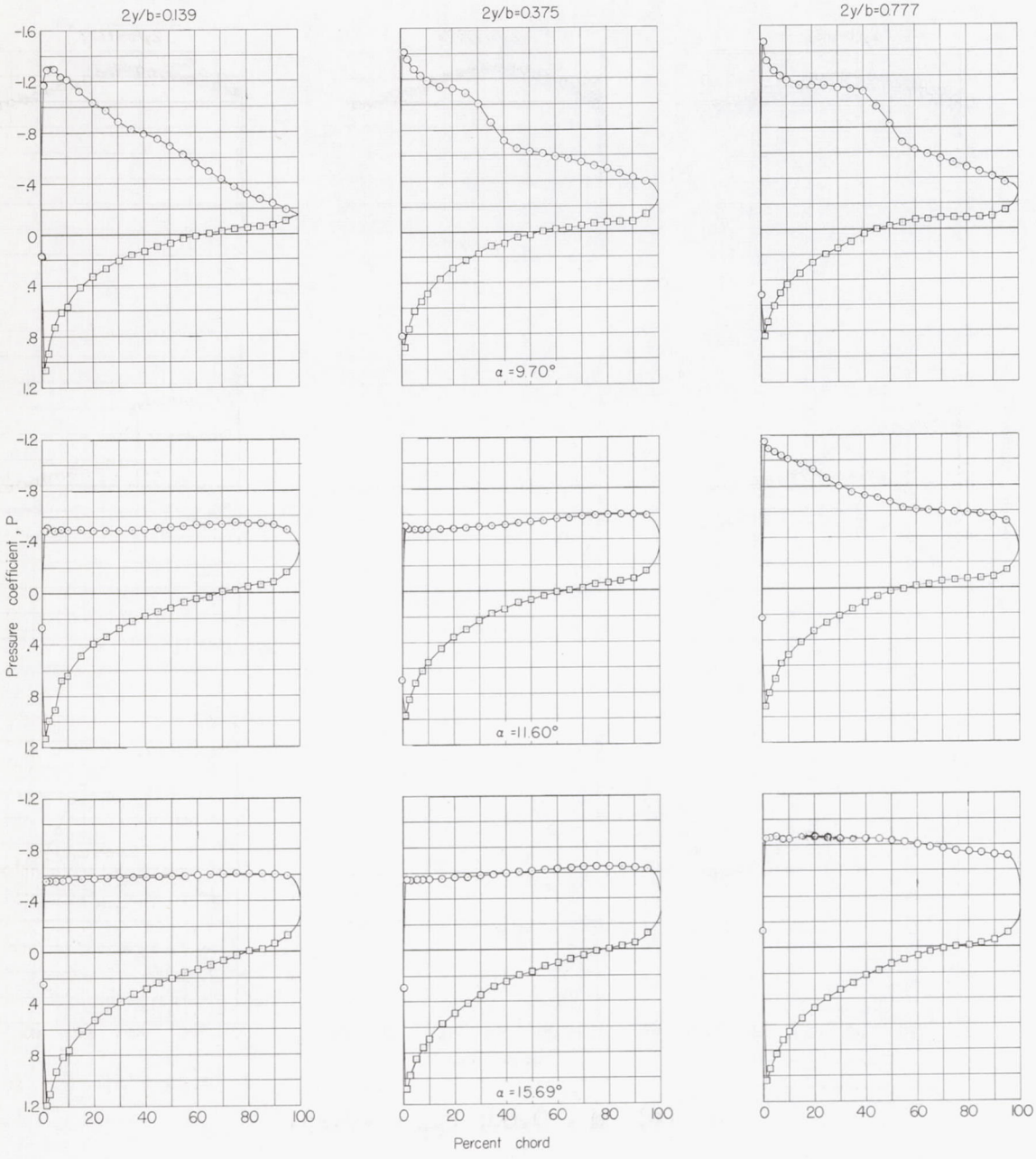

(e) Concluded.

Figure 5.- Continued.

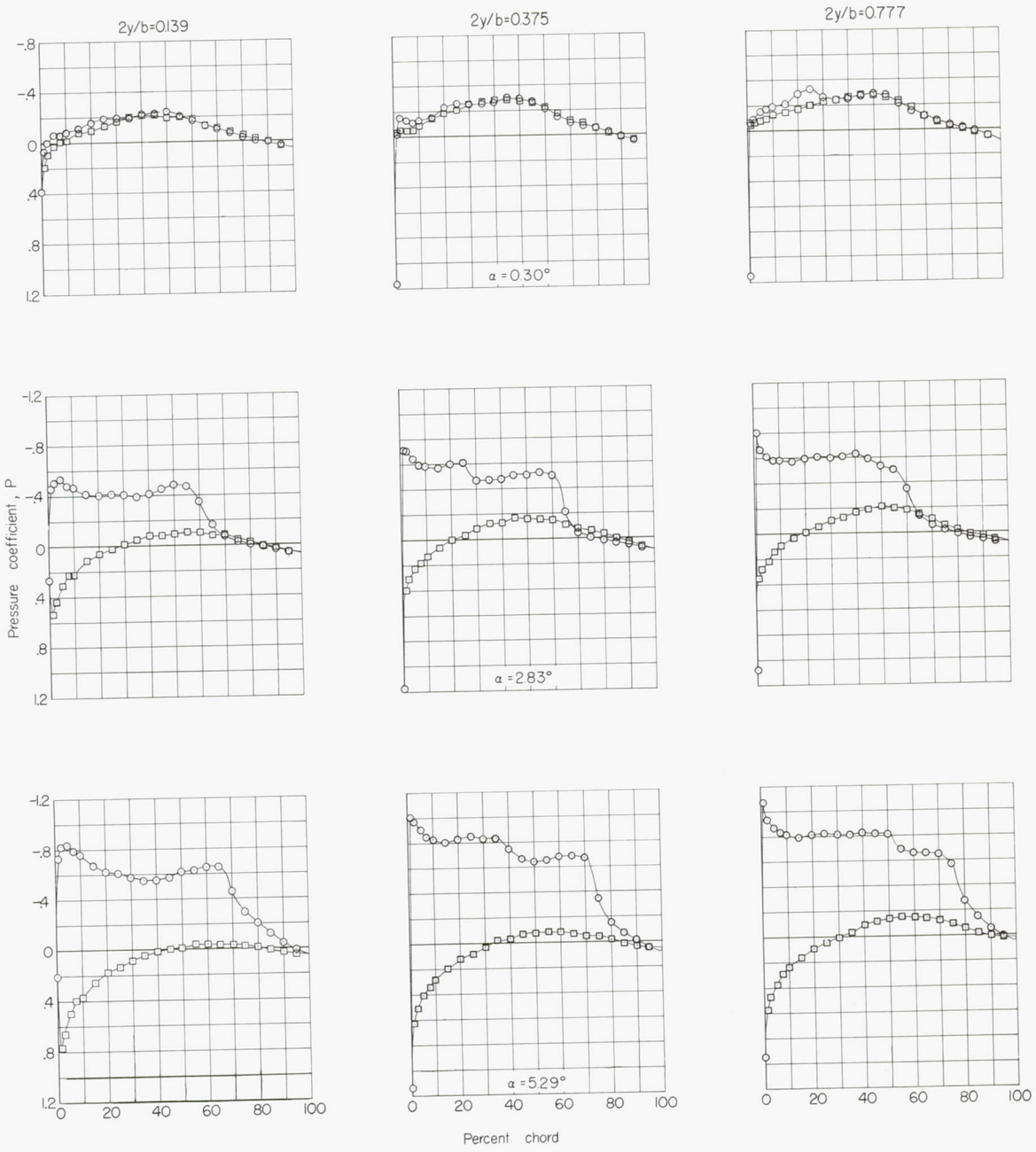

(f) M = 0.90; P_{cr} = -0.18.

Figure 5.- Continued.

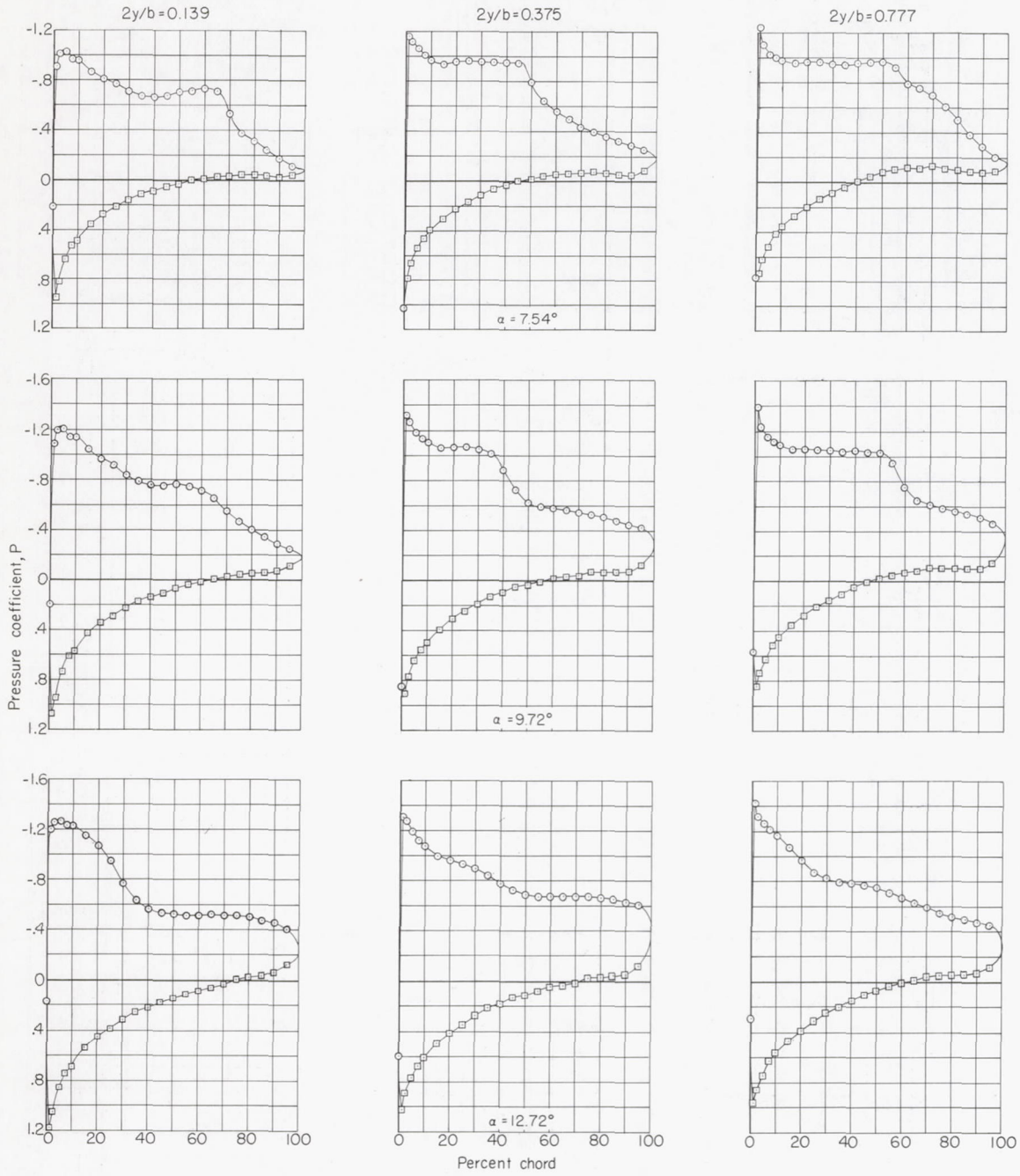

(f) Concluded.

Figure 5.- Continued.

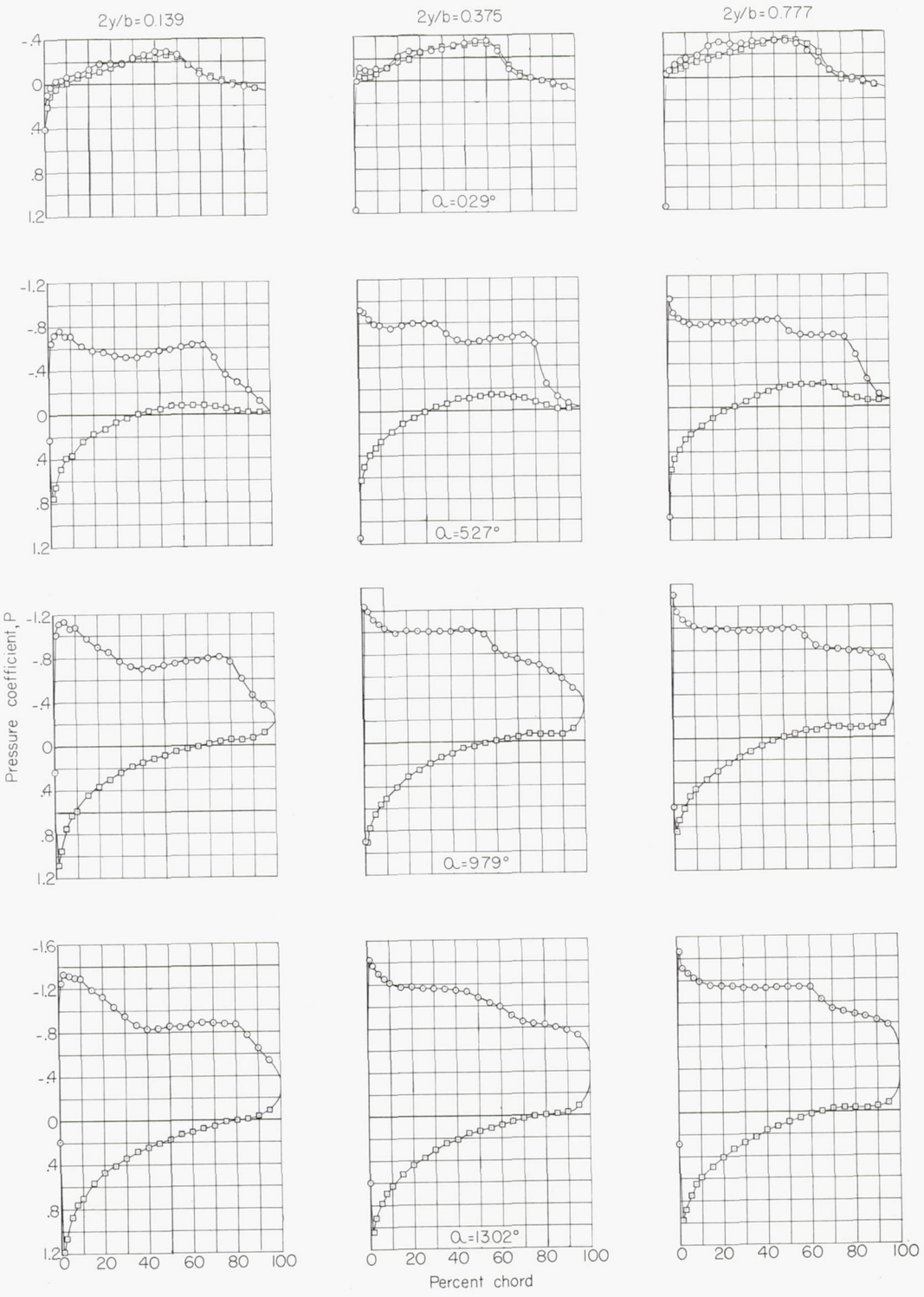

(g) M = 0.92; P_{cr} = -0.14.

Figure 5.- Continued.

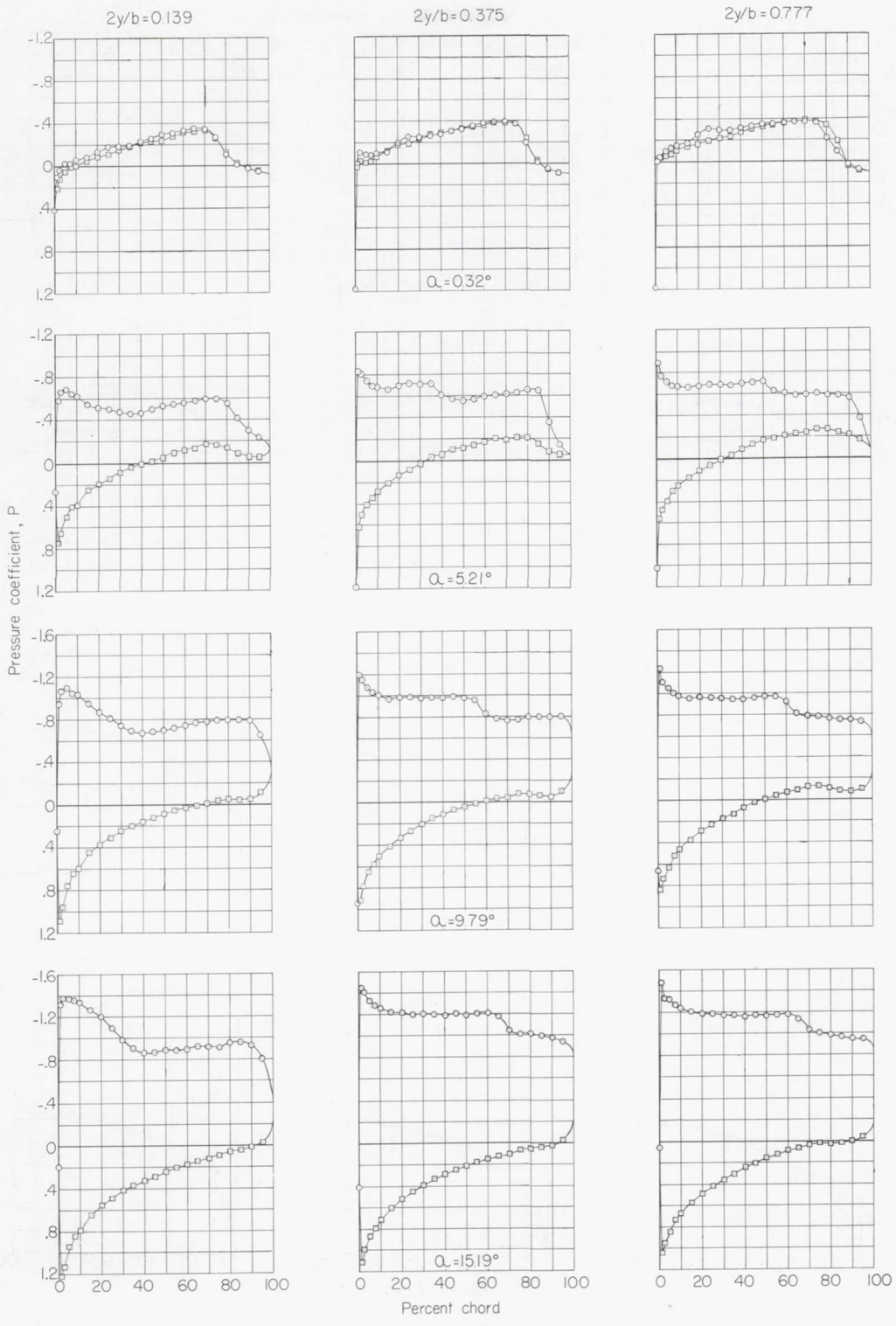

(h) M = 0.94; P_{cr} = -0.10.

Figure 5.- Continued

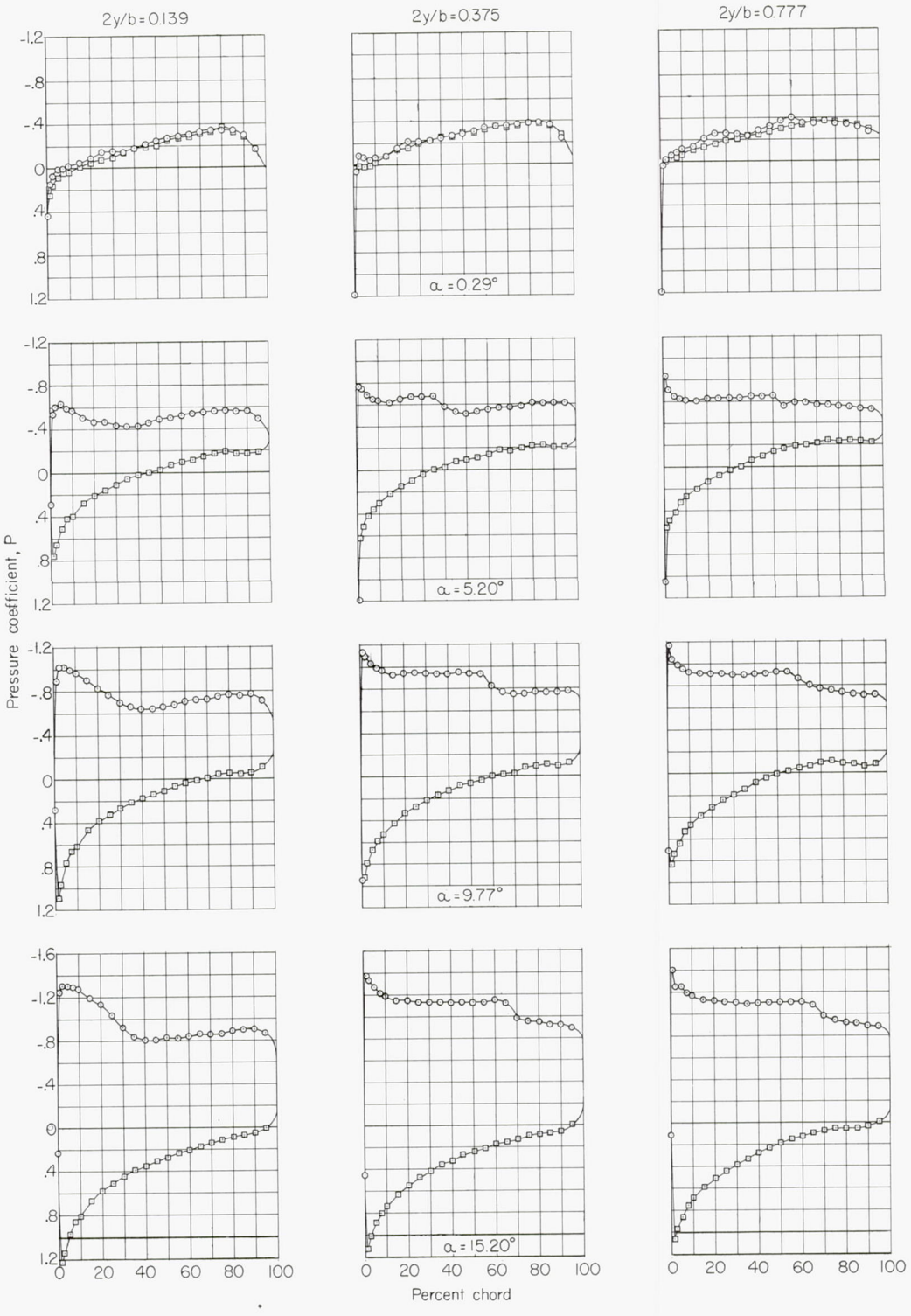

(i) M = 0.96; P_{cr} = -0.07.

Figure 5.- Continued.

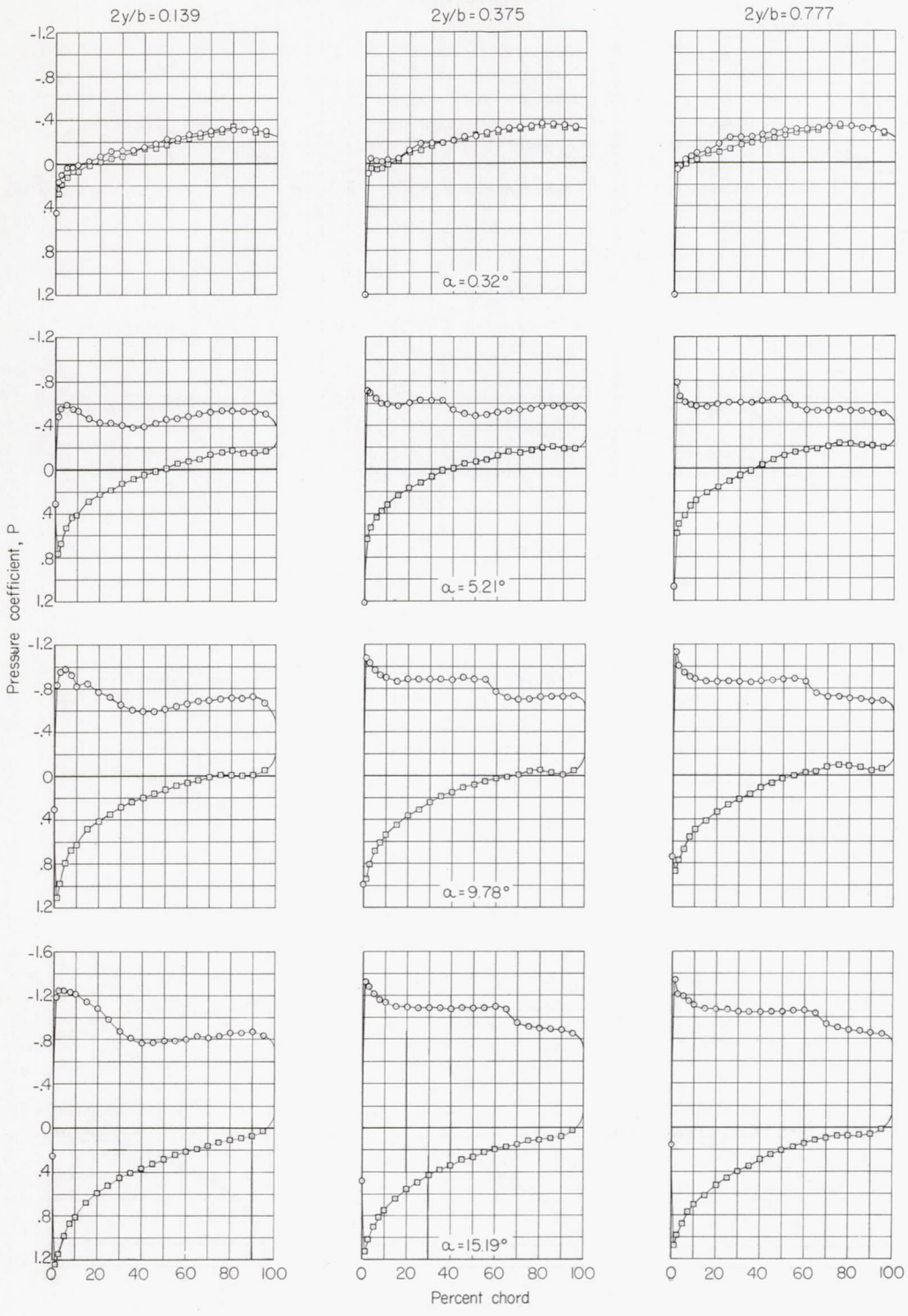

(j) $M = 0.98$; $P_{cr} = -0.03$.

Figure 5.- Continued.

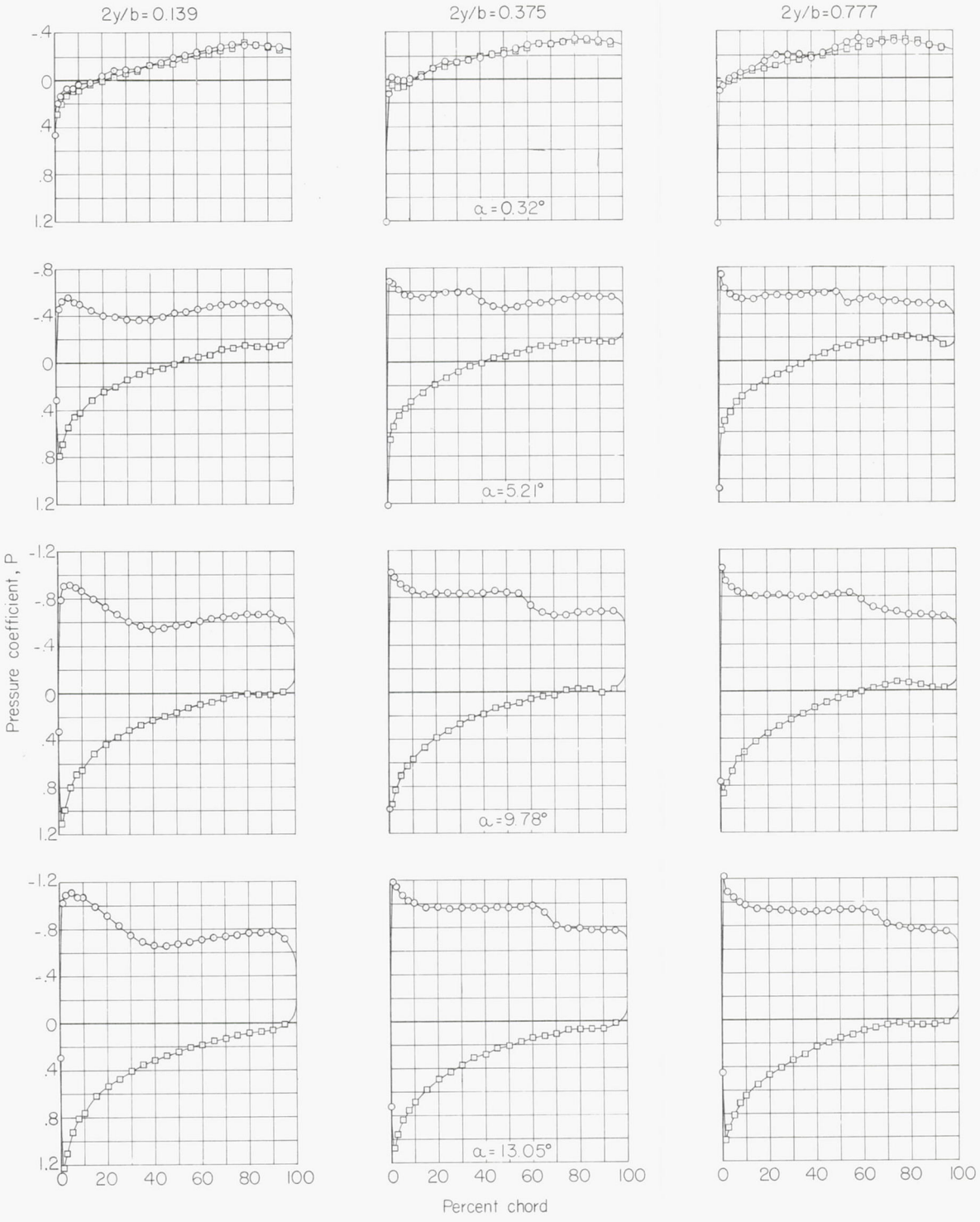

(k) M = 1.00; P_{cr} = 0.

Figure 5.- Continued.

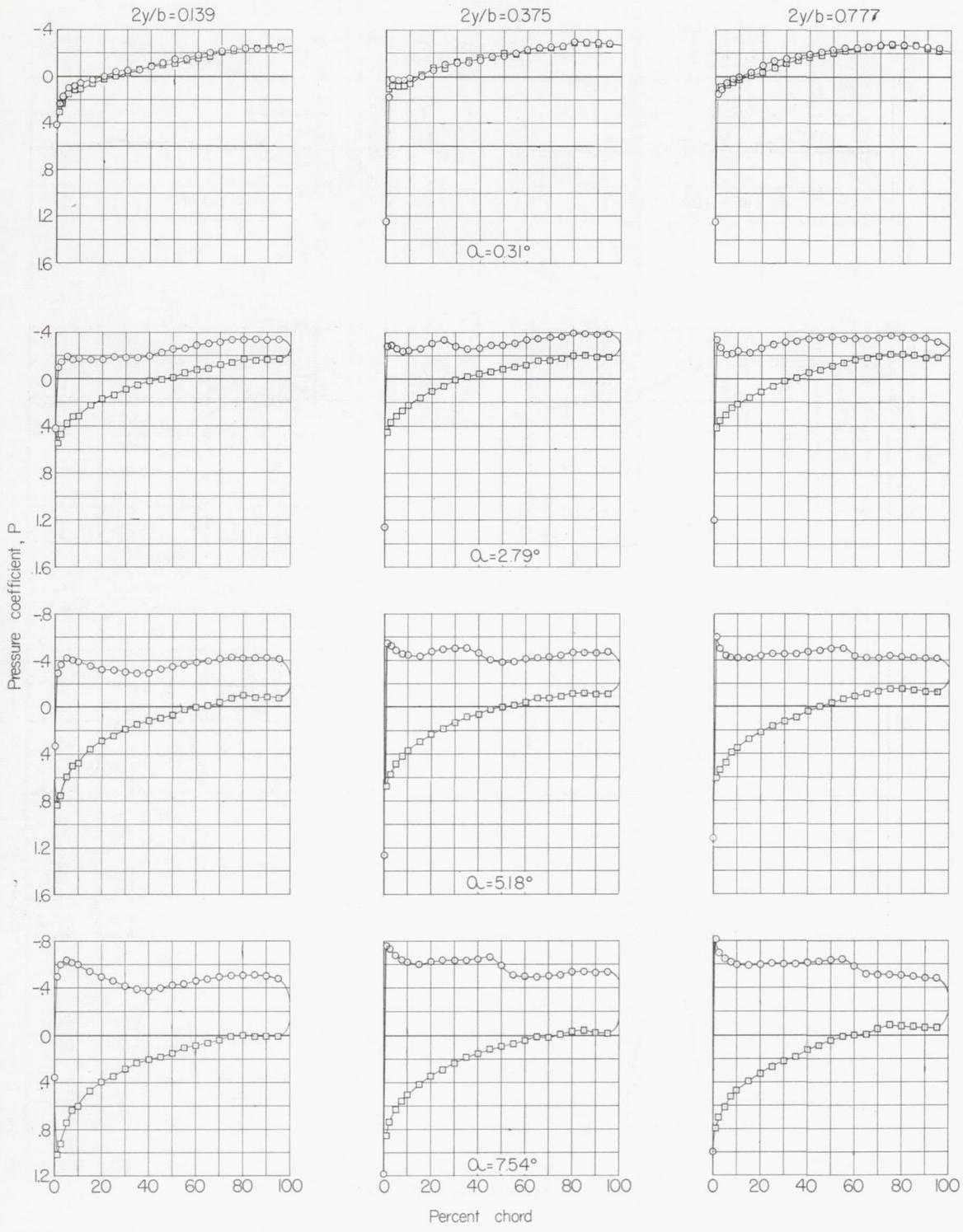

(l) M = 1.05.

Figure 5.- Concluded.

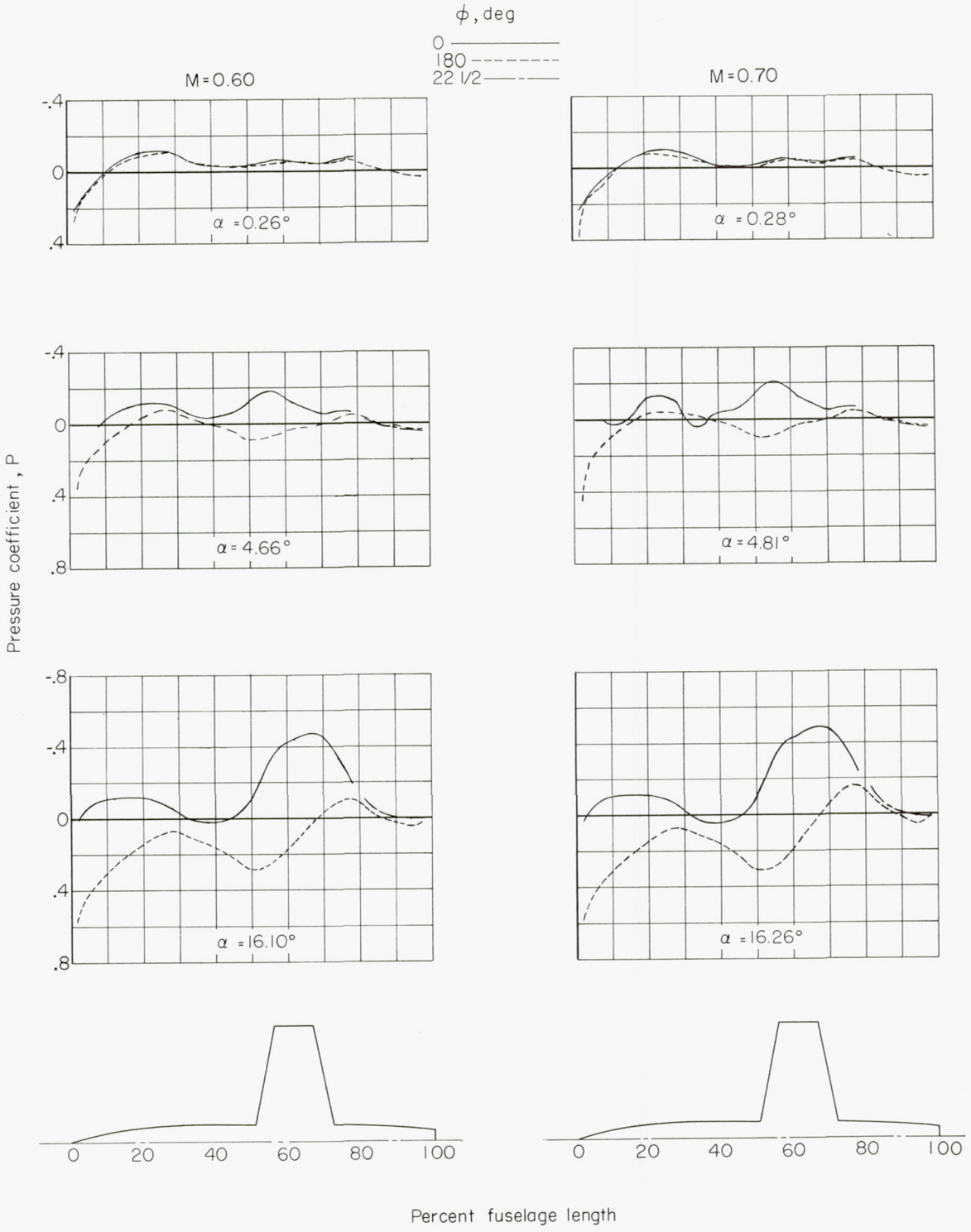

(a) M = 0.60; M = 0.70.

Figure 6.- Fuselage longitudinal pressure distributions.

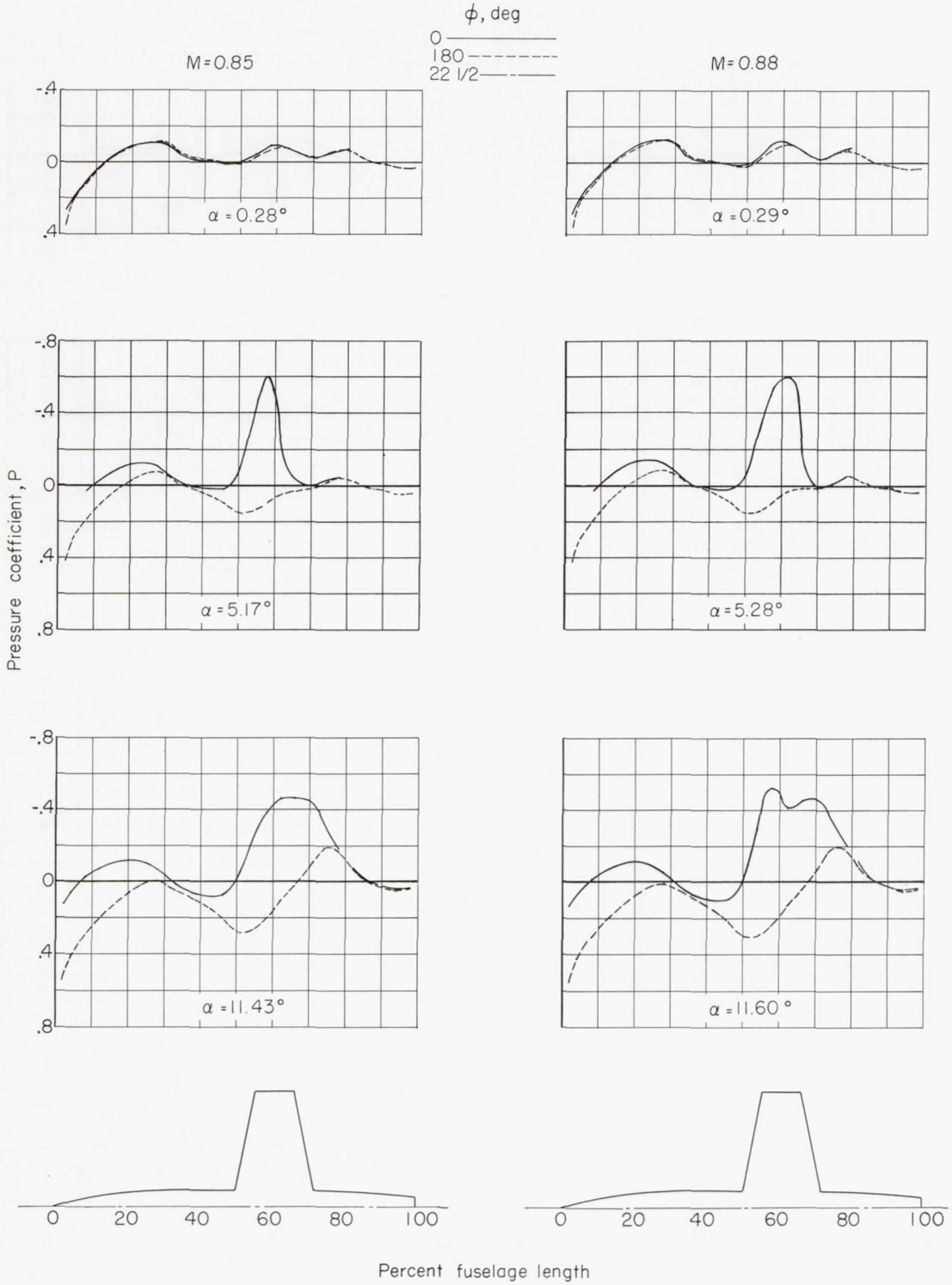

(b) M = 0.85; M = 0.88.

Figure 6.- Continued.

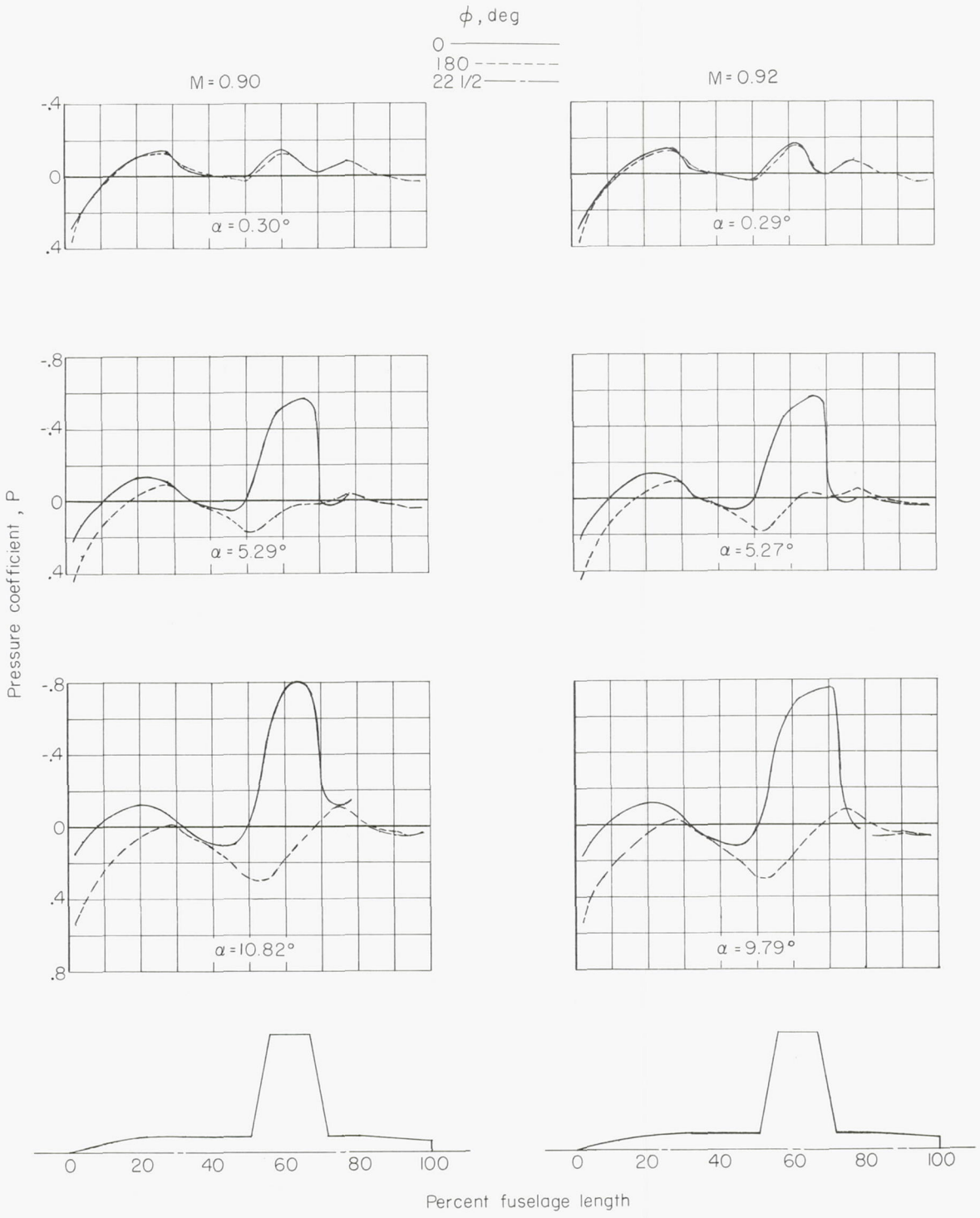

(c) M = 0.90; M = 0.92.

Figure 6.- Continued.

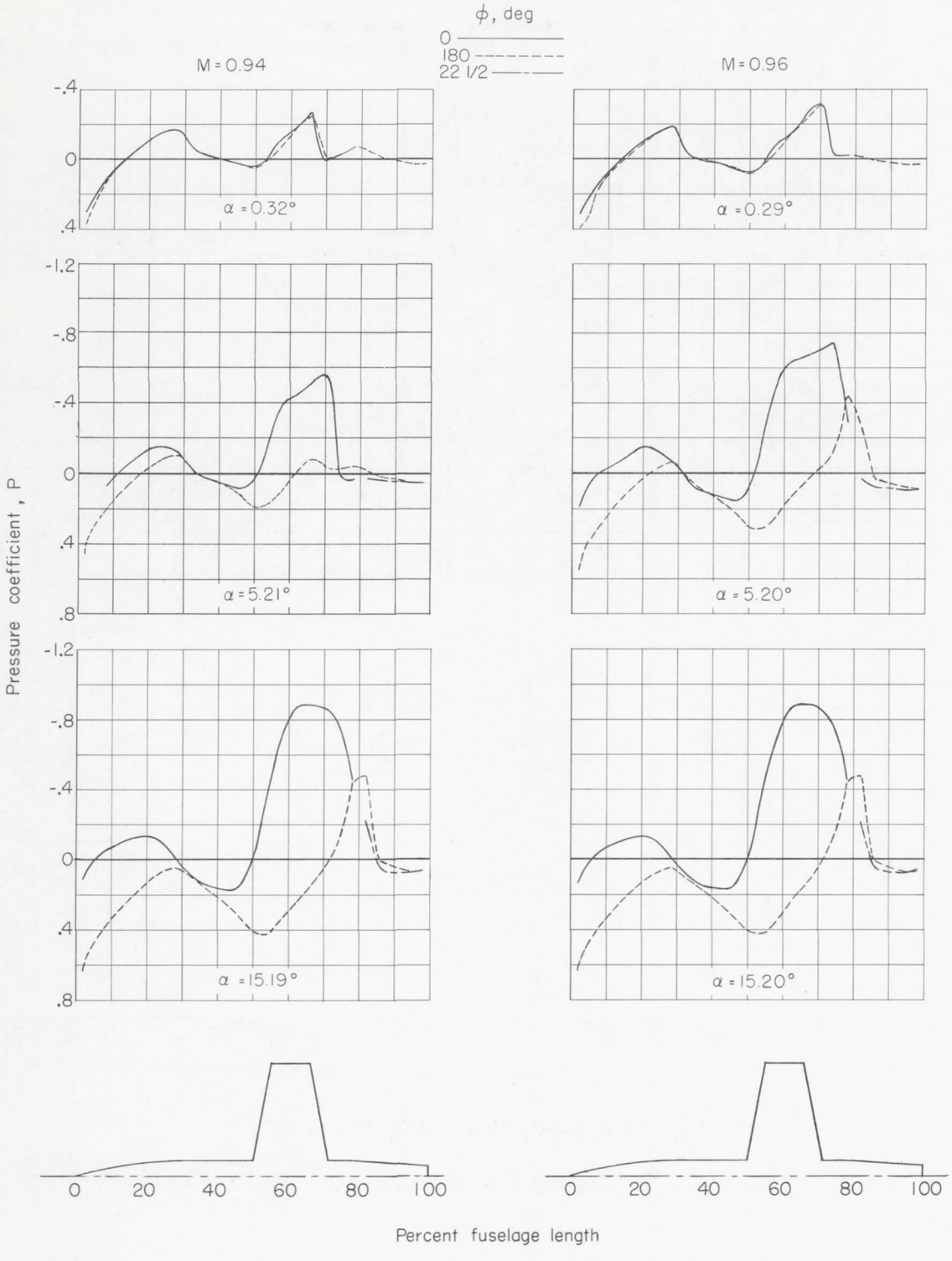

(d) M = 0.94; M = 0.96.

Figure 6.- Continued.

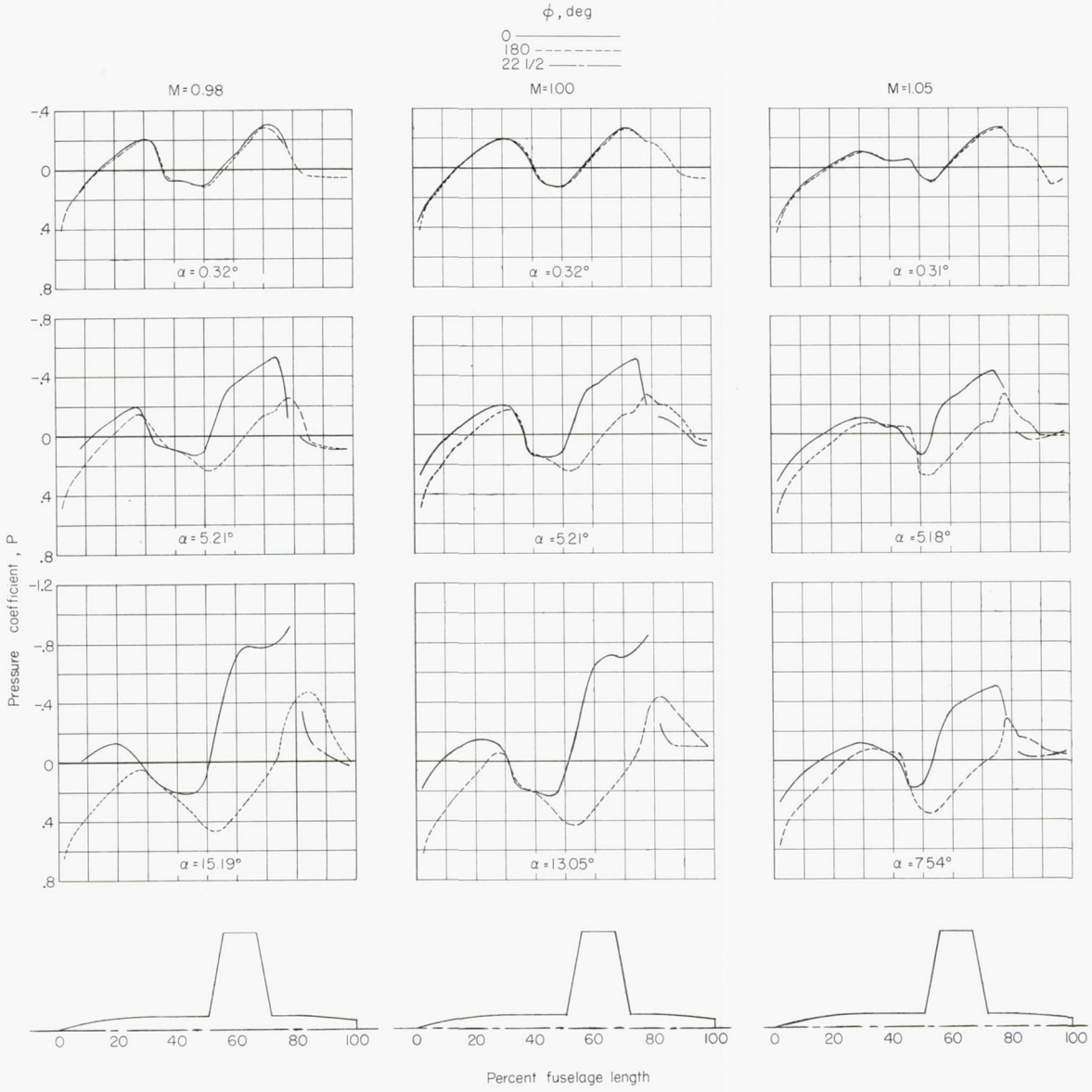

(e) M = 0.98; M = 1.00; M = 1.05.

Figure 6.- Concluded.

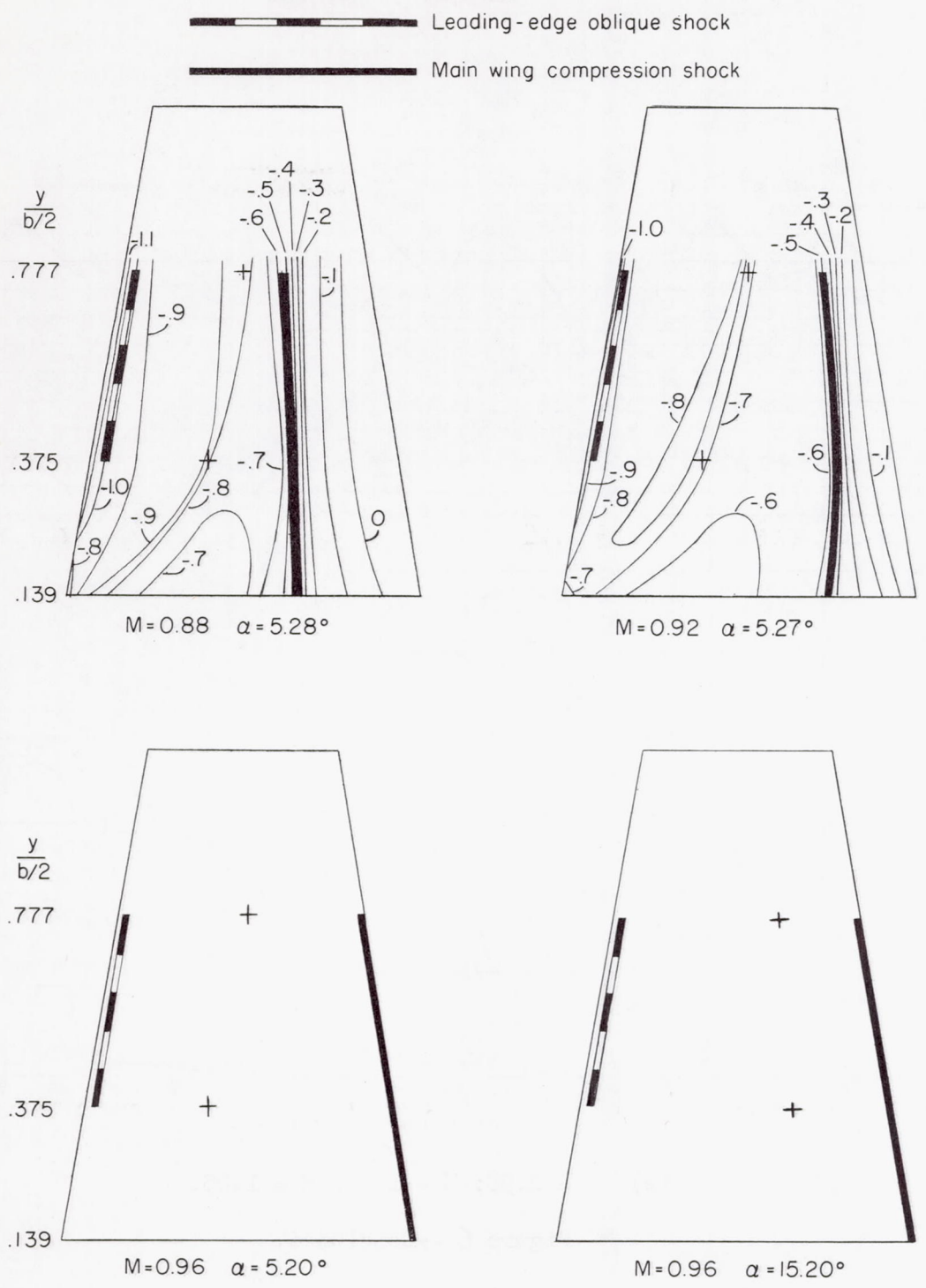

Figure 7.- Plan-form view of shocks occurring on upper surface of wing at transonic speeds. Cross marks denote location of oblique shocks caused by disturbances at wing-fuselage leading-edge juncture and wing tip. Isobars are shown in terms of upper-surface pressure coefficient P.

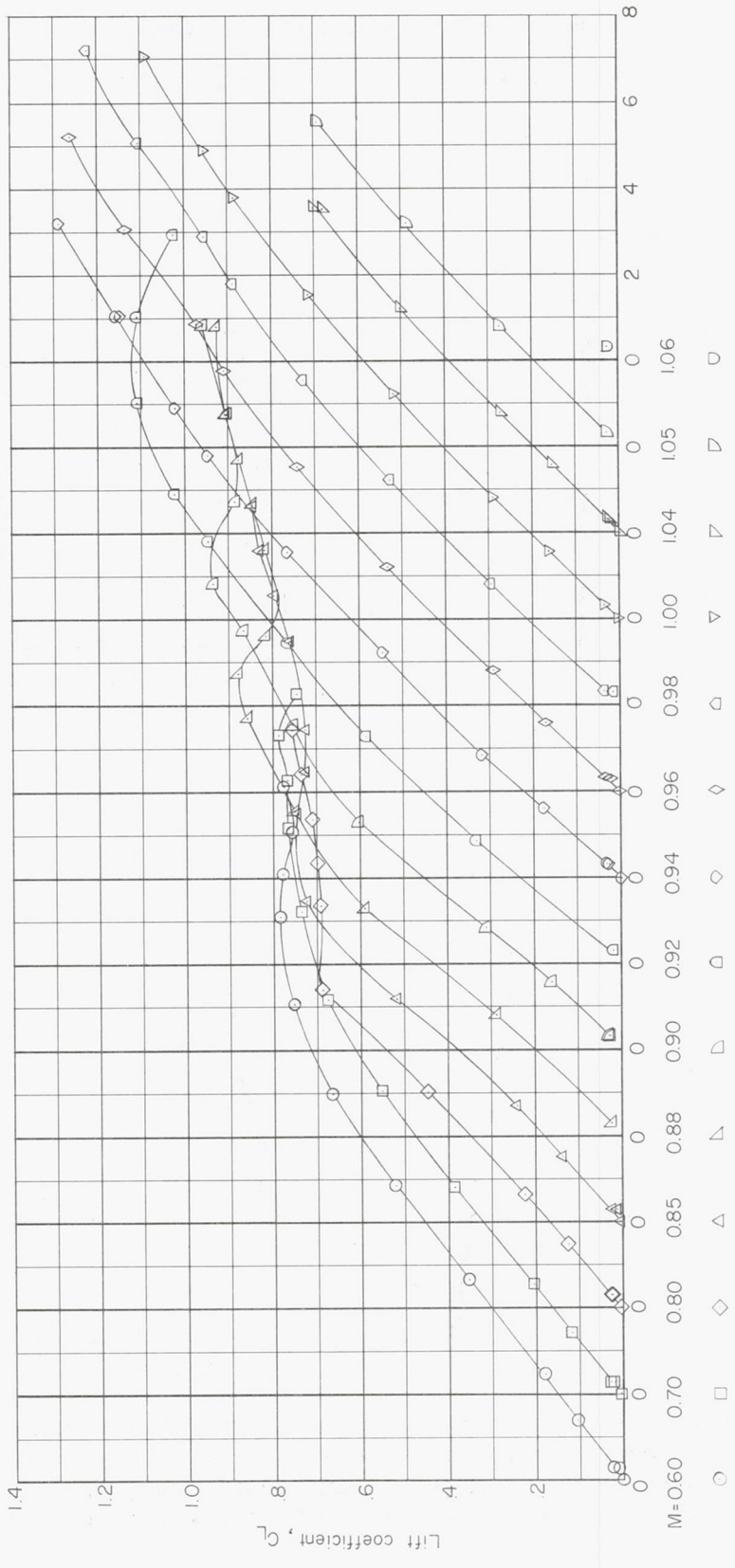

Figure 8.- Lift characteristics.

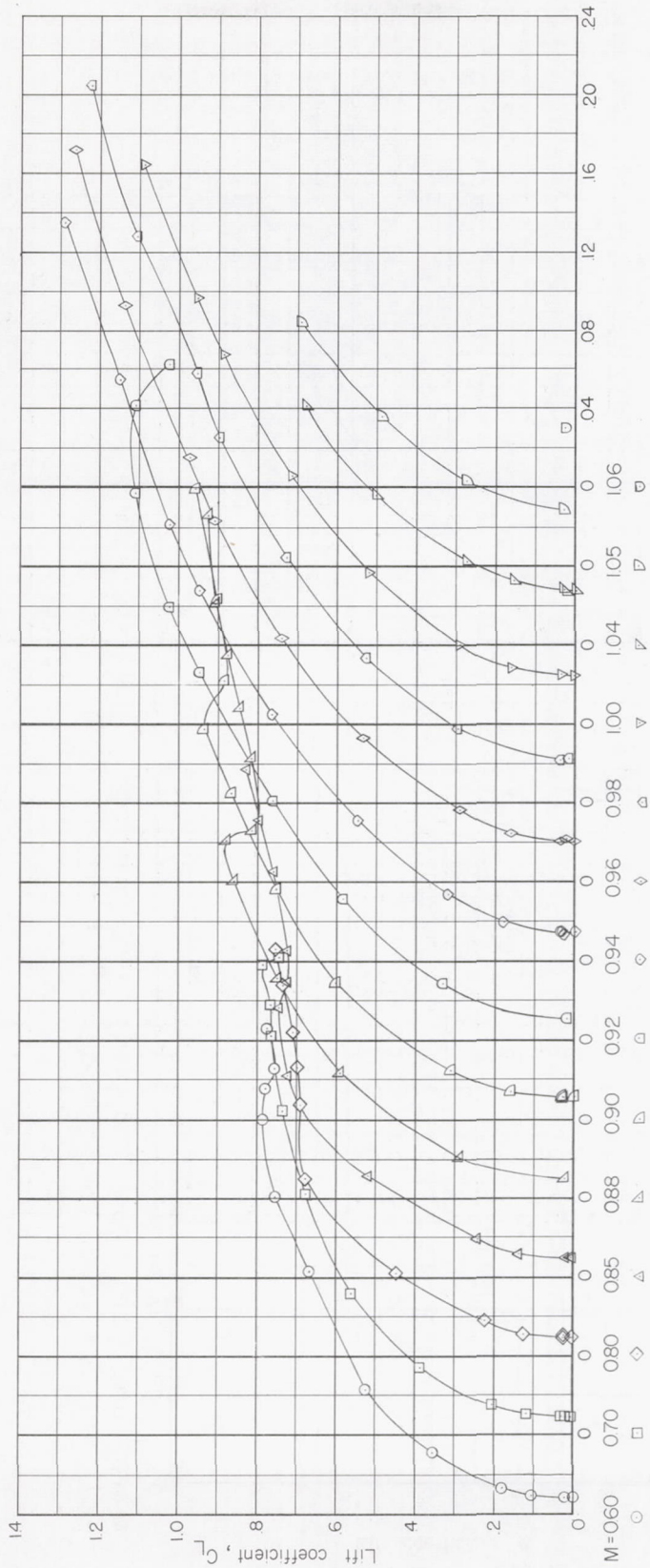

Figure 9.- Drag characteristics.

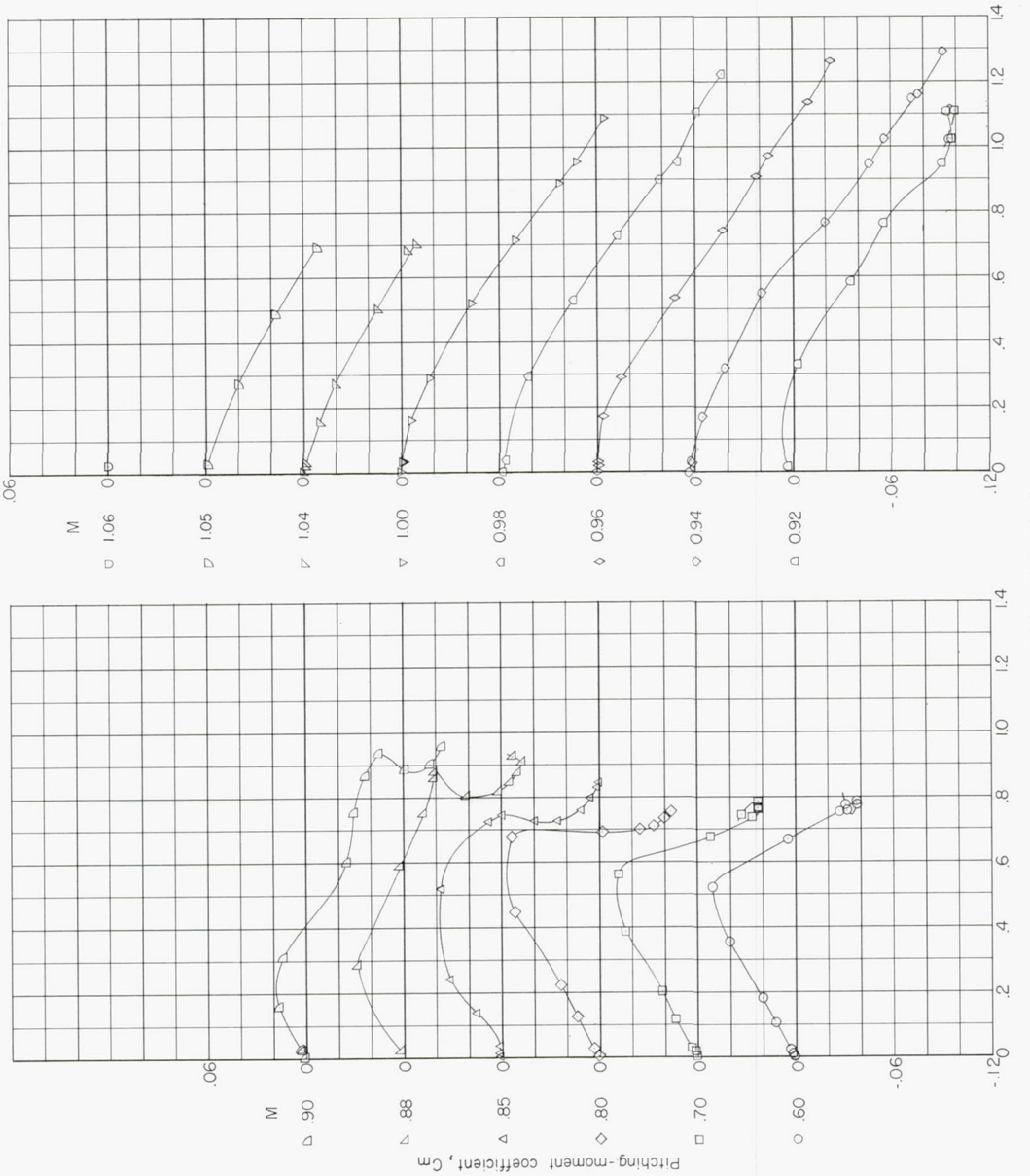

Figure 10.- Pitching-moment characteristics.

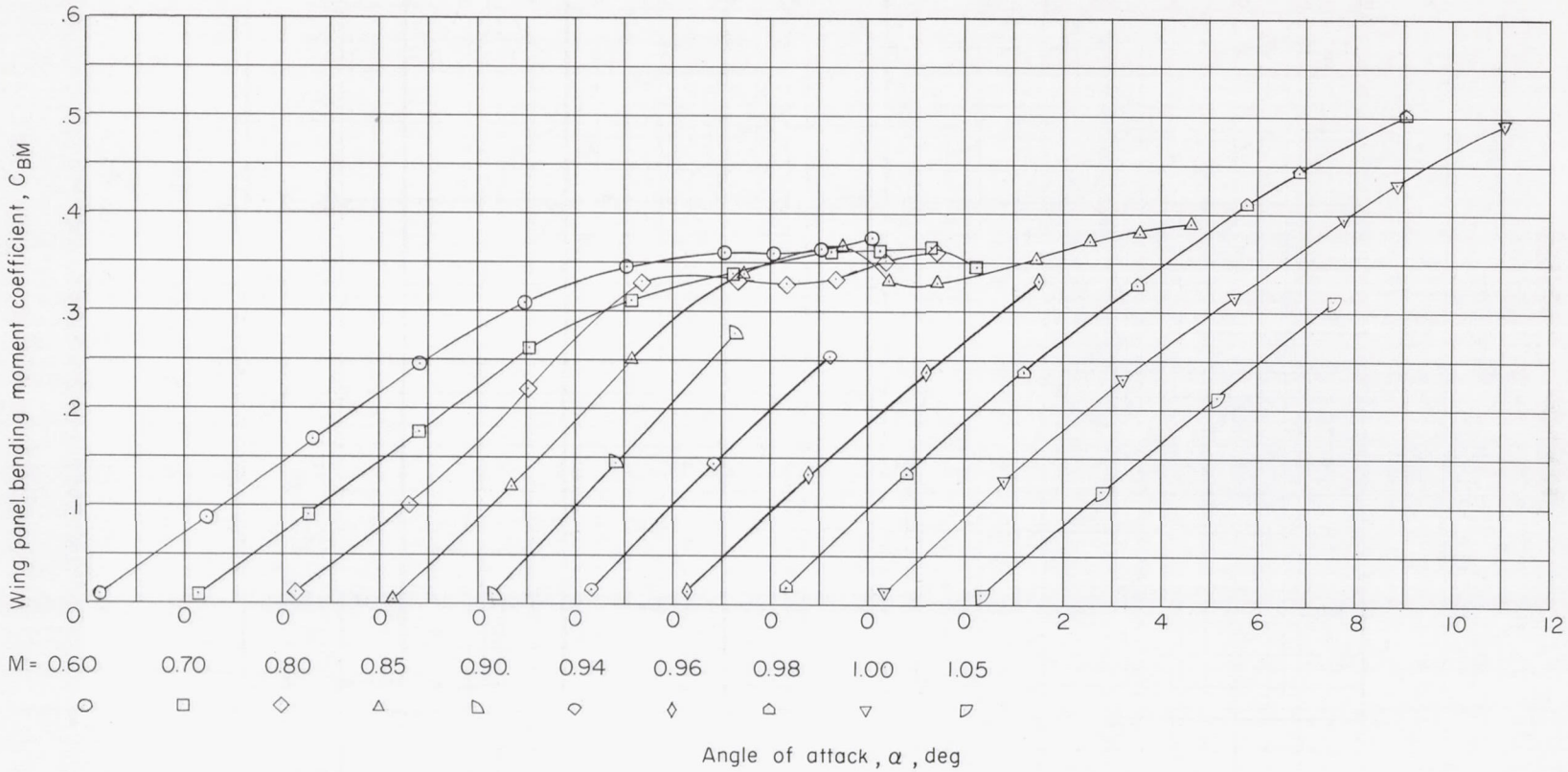

Figure 11.- Variation of wing-panel bending-moment coefficient with angle of attack for various Mach numbers.

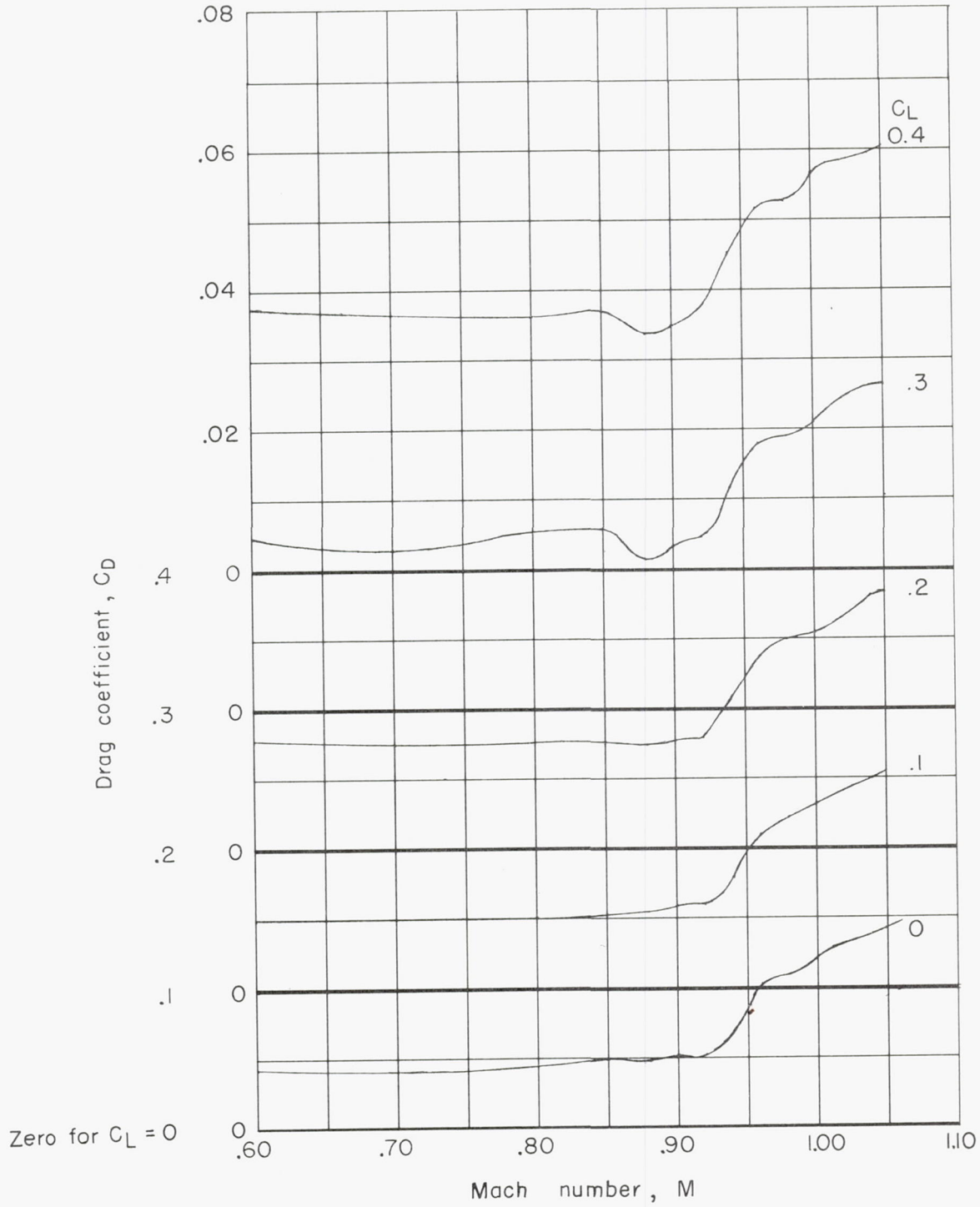

Figure 12.- Effect of Mach number on drag coefficient at constant values of lift coefficient.

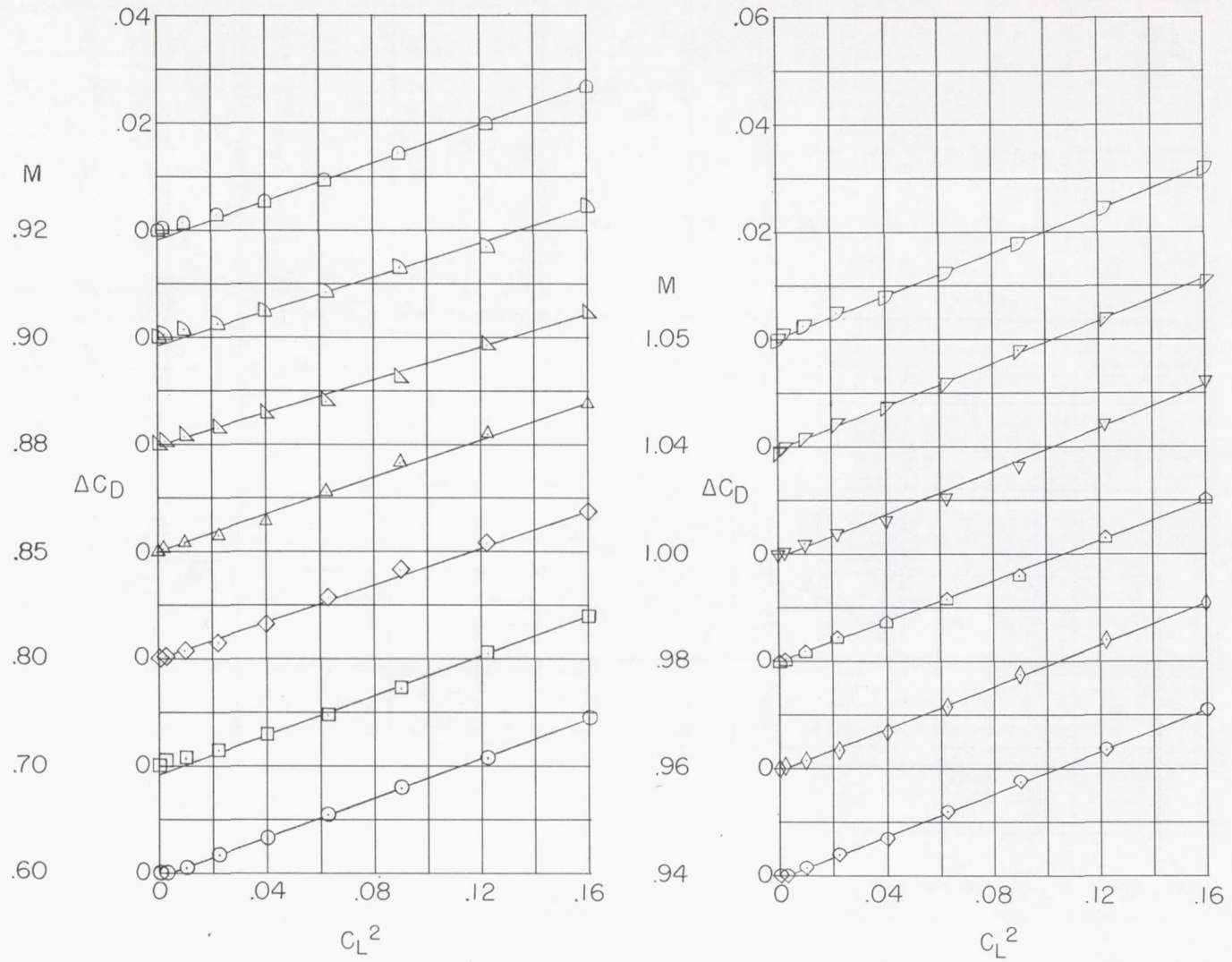

Figure 13.- Variation of total drag coefficient minus zero-lift drag coefficient with square of lift coefficient for various Mach numbers.

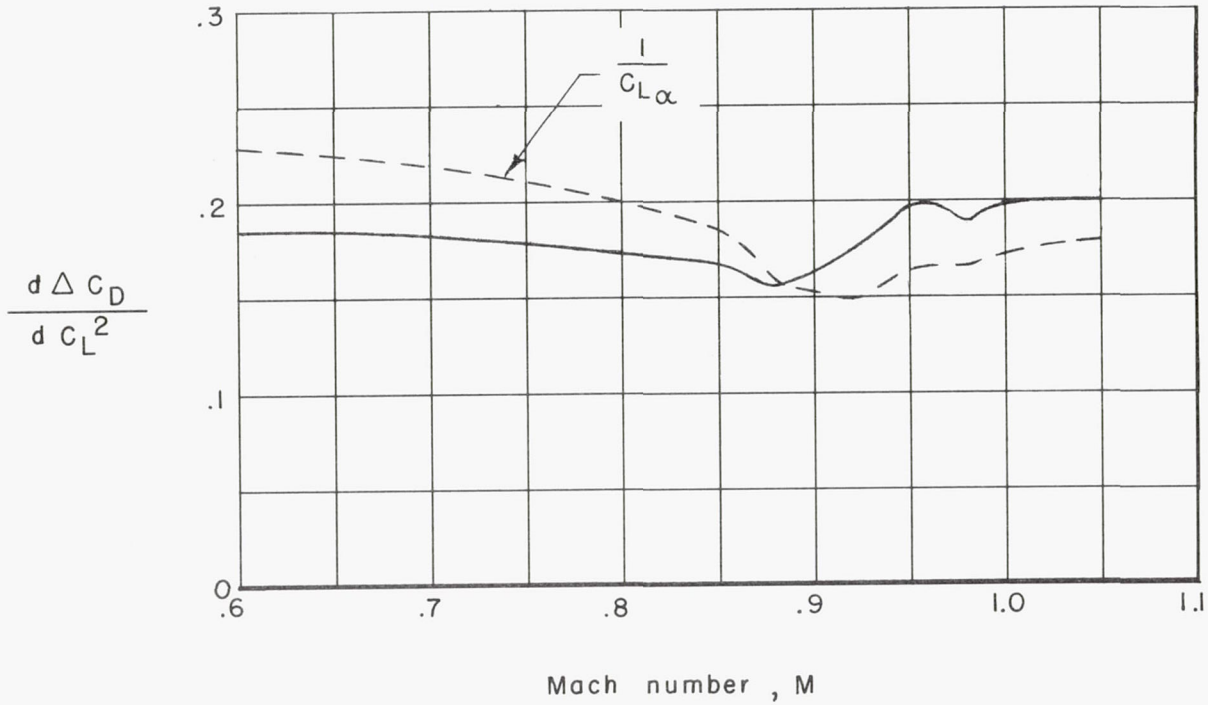

Figure 14.- Effect of Mach number on drag due to lift parameter.

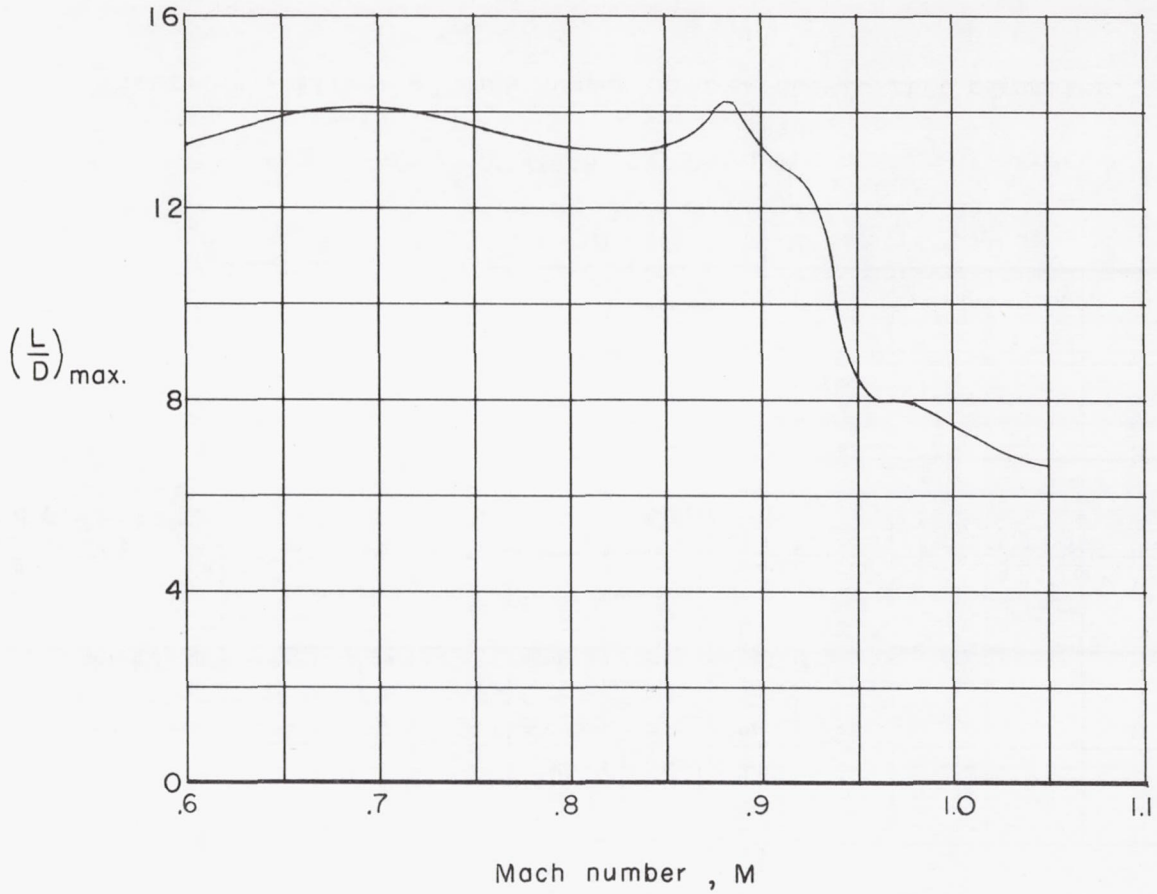

Figure 15.- Effect of Mach number on maximum lift-drag ratio.

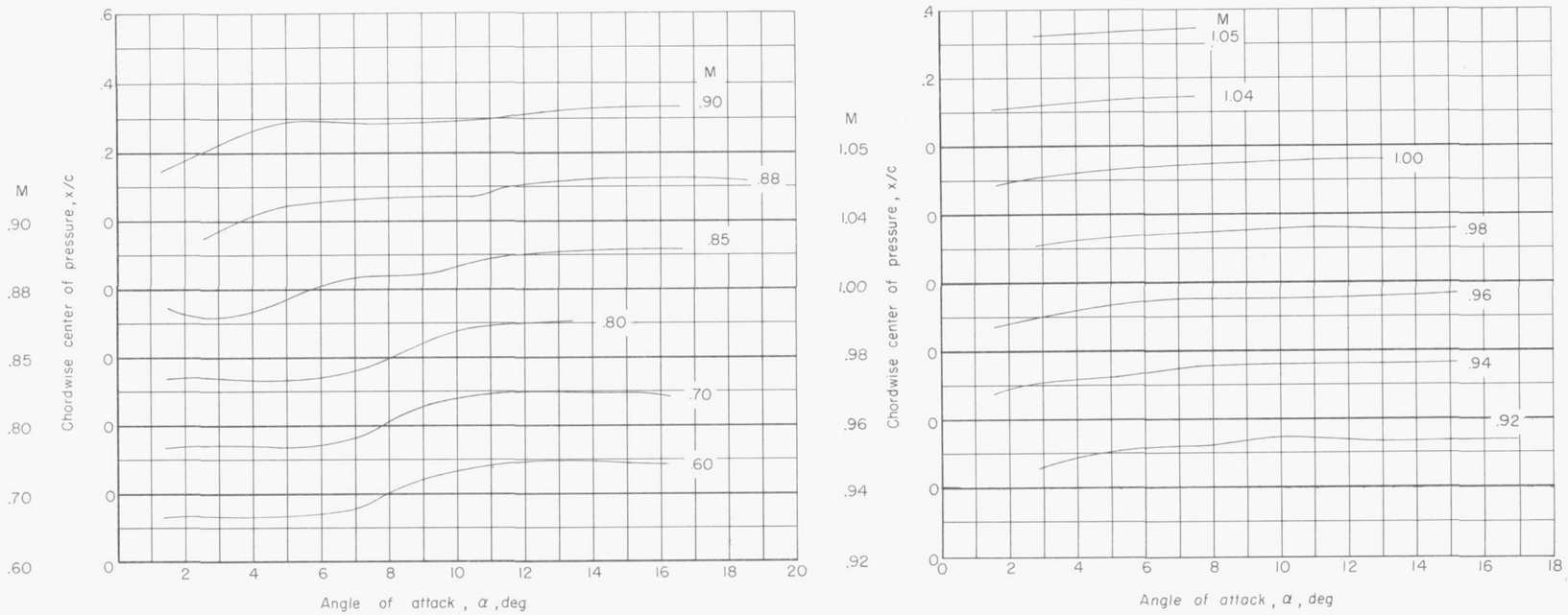

Figure 16.- Effect of angle of attack of chordwise center-of-pressure position at various Mach numbers.

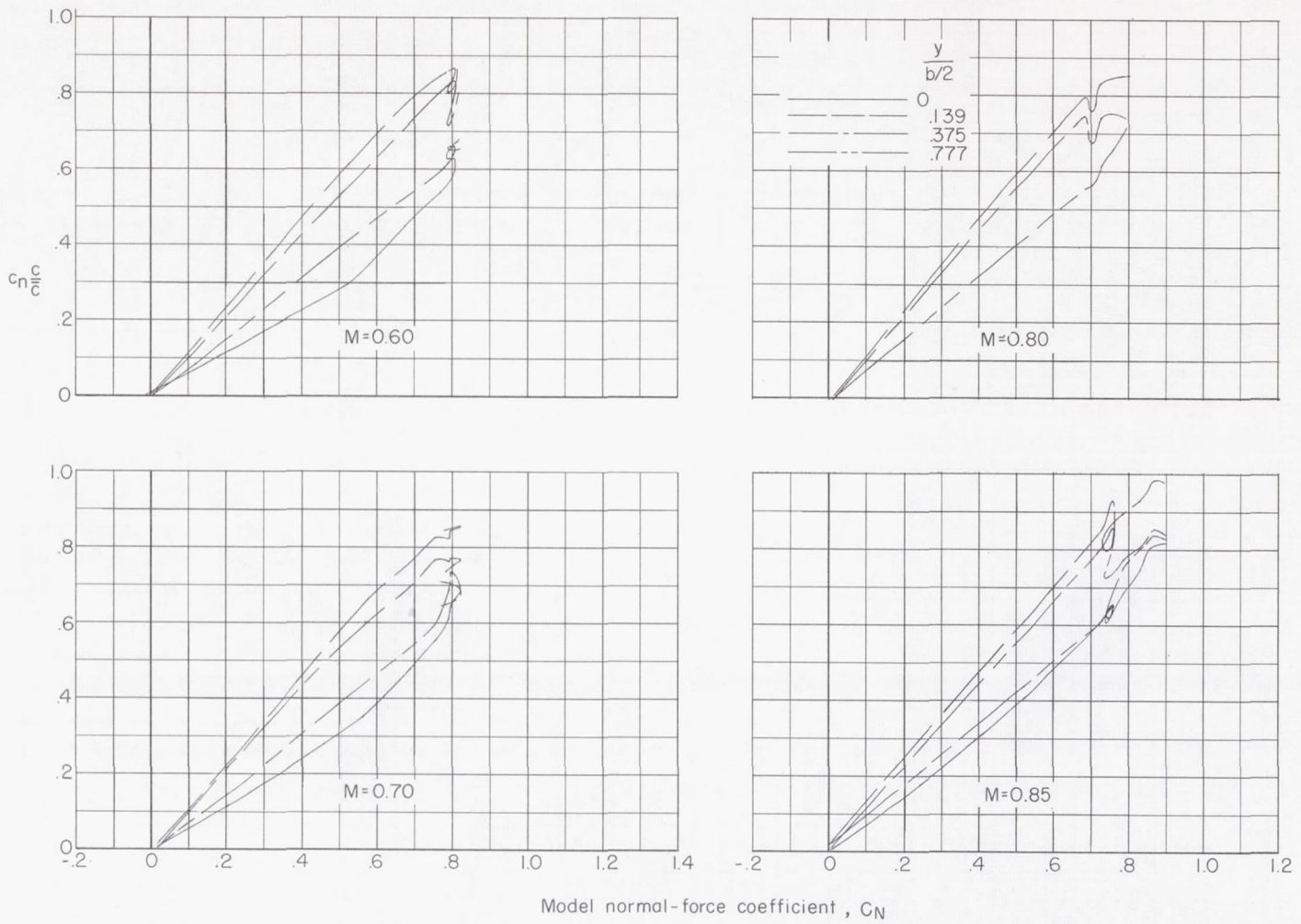

(a) M = 0.60, 0.70, 0.80, 0.85.

Figure 17.- Variation of section normal-load coefficient with model normal-force coefficient for various Mach numbers.

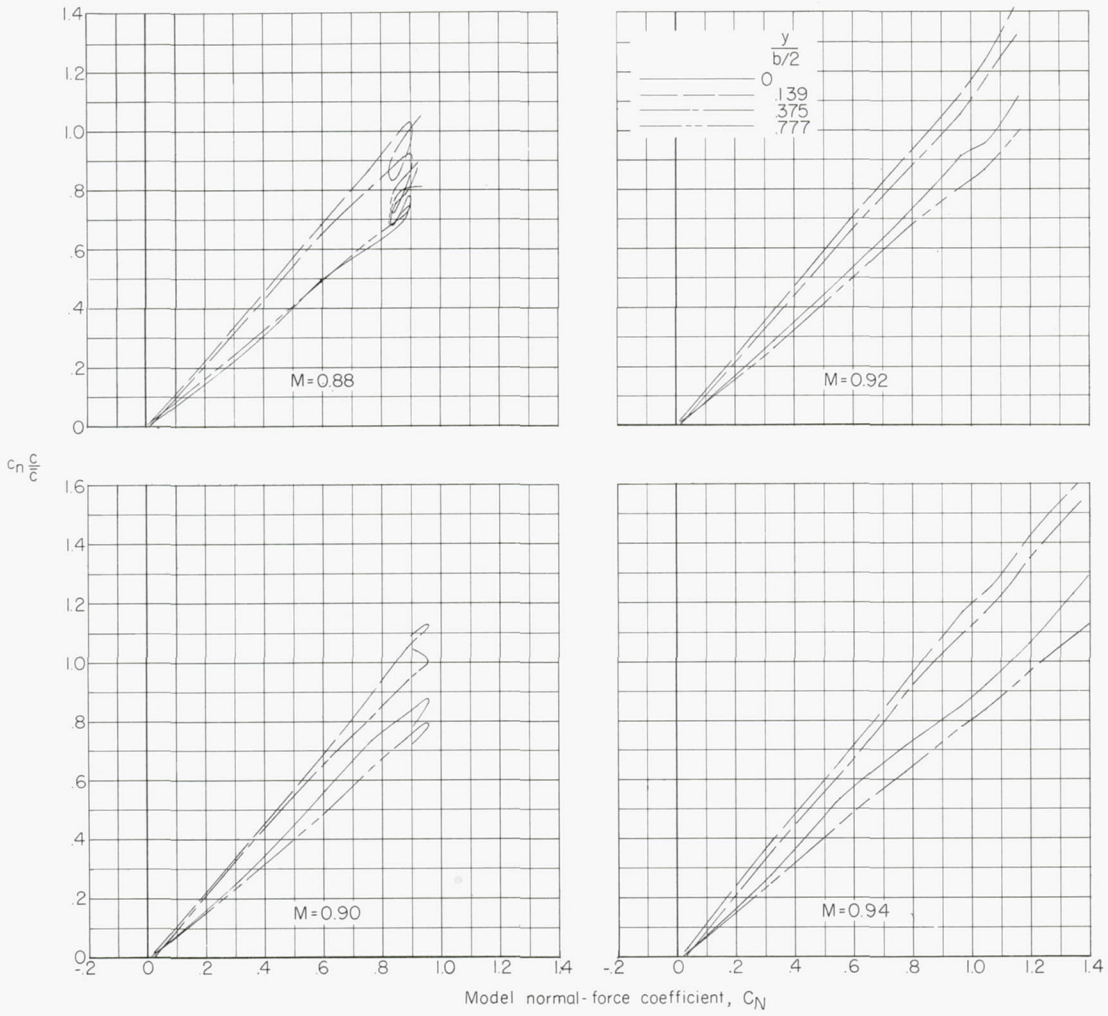

(b) M = 0.88, 0.90, 0.92, 0.94.

Figure 17.- Continued.

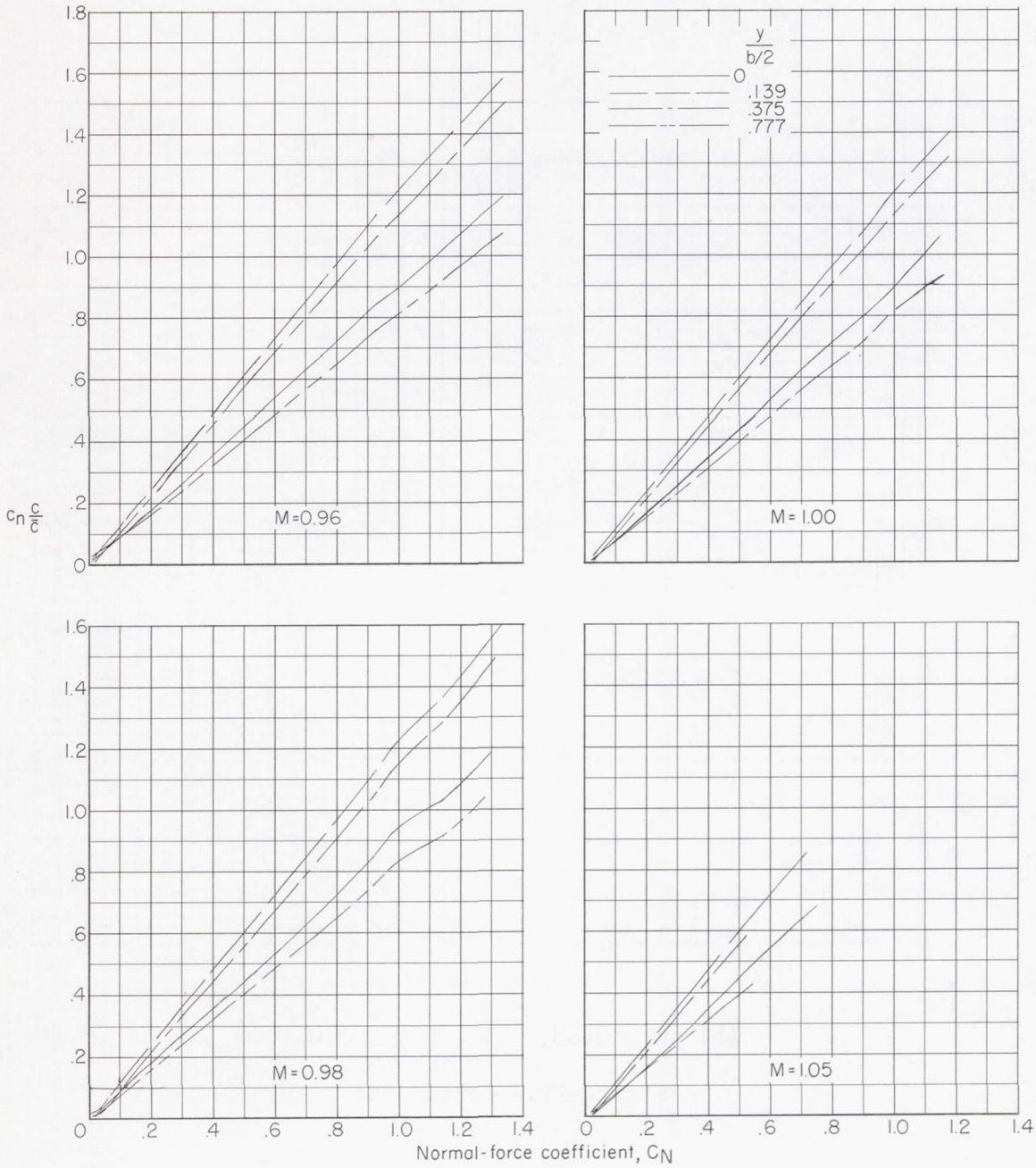

(c) M = 0.96, 0.98, 1.00, 1.05.

Figure 17.- Concluded.

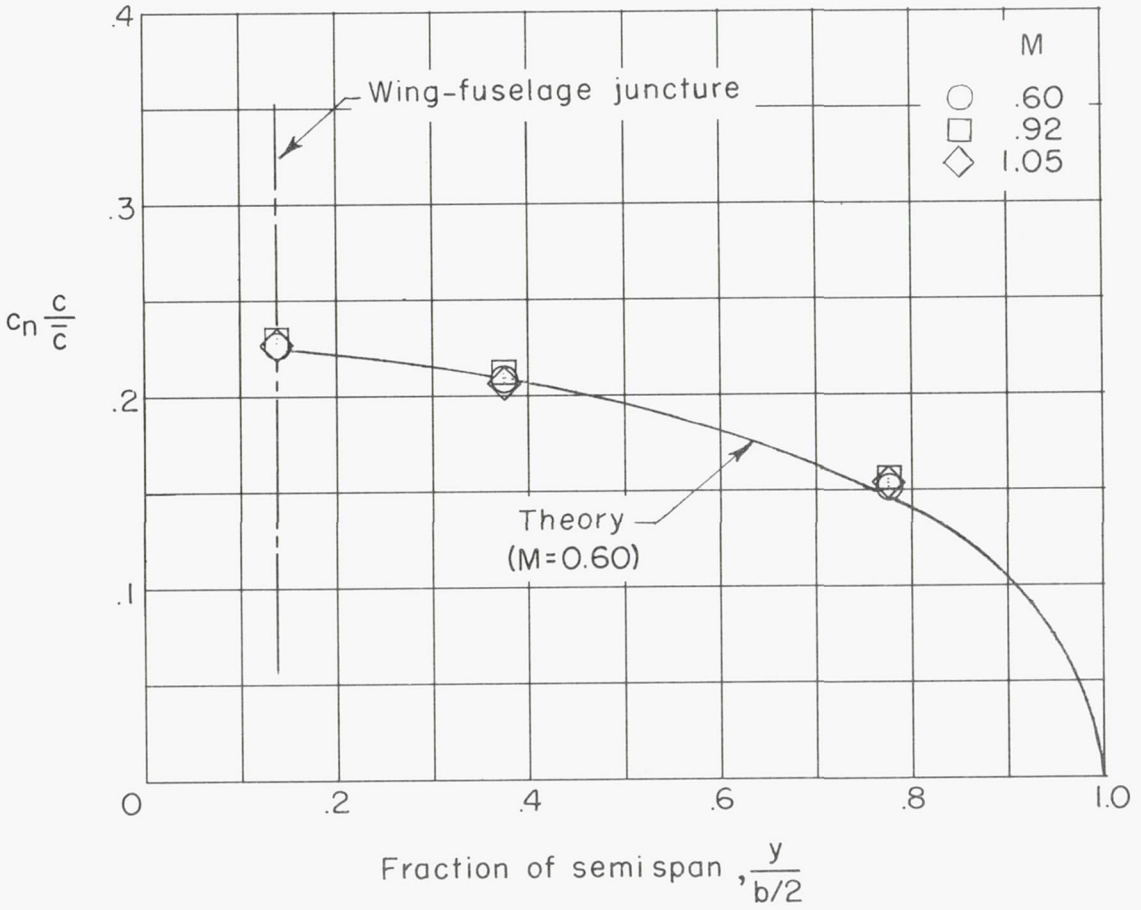

Figure 18.- Comparison of span load distributions of the model $\left(C_N = 0.2\right)$ with theory.

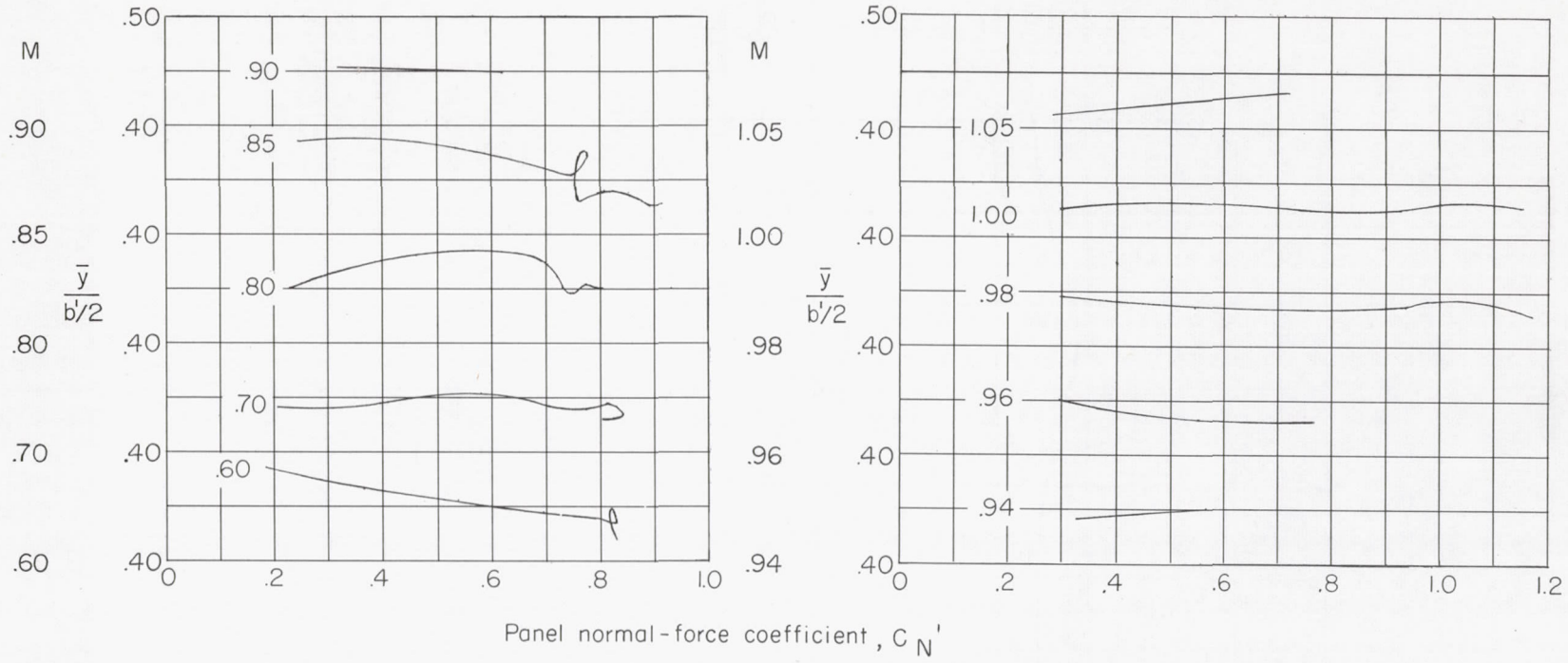

Figure 19.- Effect of panel normal-force coefficient on spanwise center of load parameter at various Mach numbers.

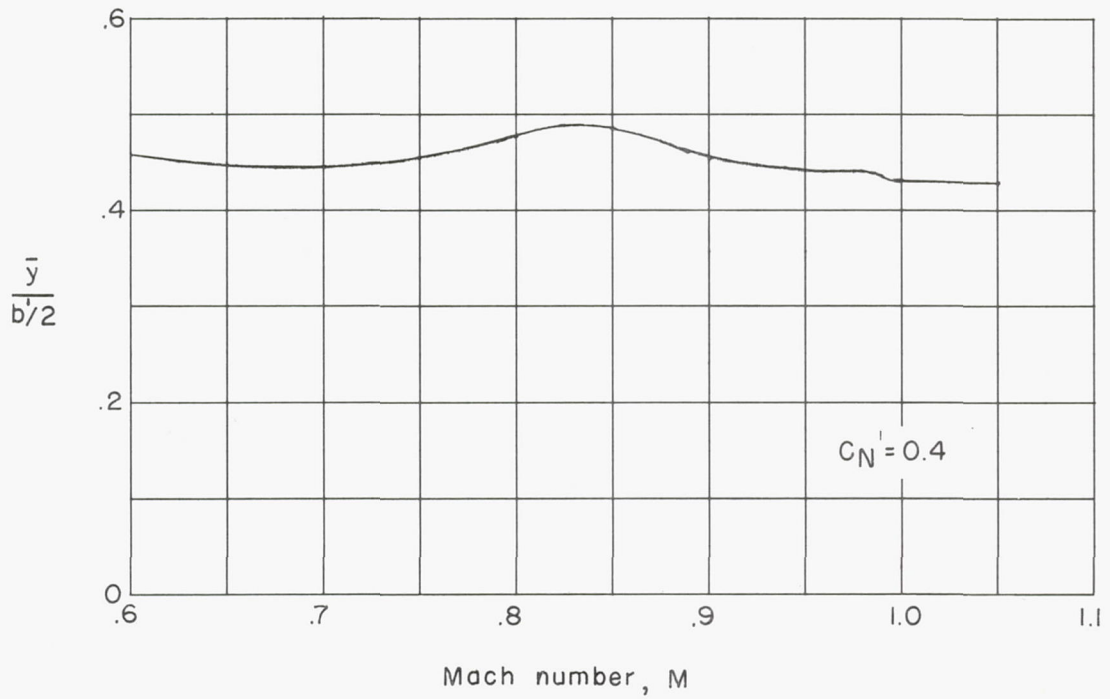

Figure 20.- Effect of Mach number on spanwise center of load parameter at a panel normal-force coefficient of 0.4.

NACA-Langley - 5-24-54 - 325